NUCLEAR DATA AND MEASUREMENTS SERIES

ANL/NDM-90

Fast-Neutron-Spectrum Measurements for the Thick-Target $^{9}Be(d,n)^{10}B$ Reaction at E_d = 7 MeV

by

D.L. Smith, J.W. Meadows, and P.T. Guenther

April 1985

ARGONNE NATIONAL LABORATORY,
ARGONNE, ILLINOIS 60439, U.S.A.

NUCLEAR DATA AND MEASUREMENTS SERIES

ANL/NDM-90

FAST-NEUTRON-SPECTRUM MEASUREMENTS FOR THE THICK-TARGET $^{9}Be(d,n)^{10}B$ REACTION AT E_d = 7 MeV

by

D. L. Smith, J. W. Meadows and P. T. Guenther

April 1985

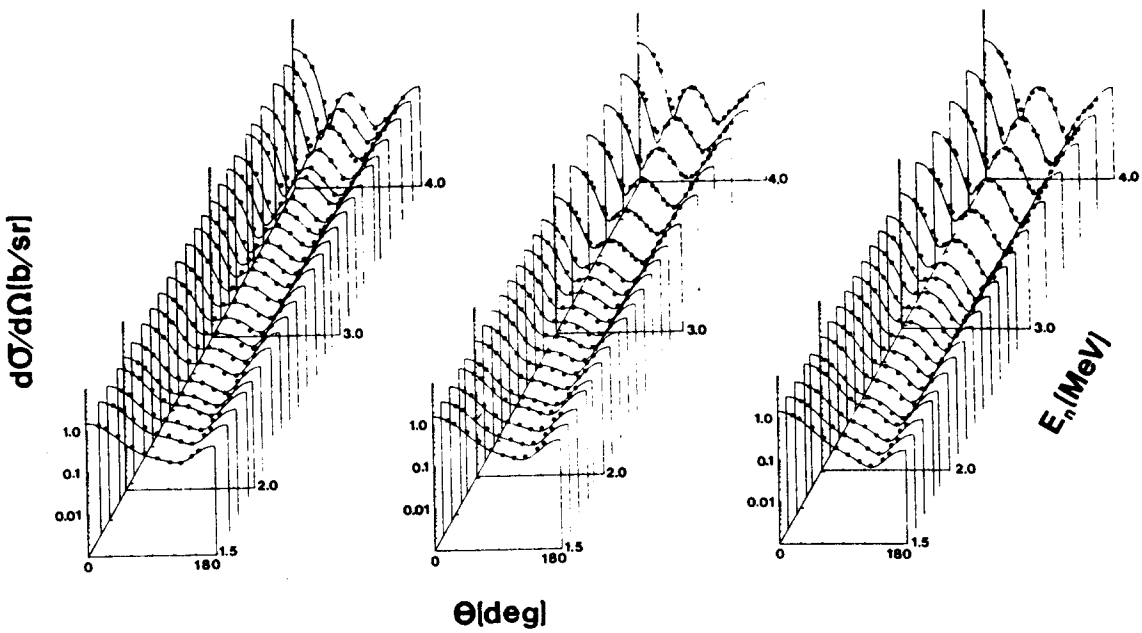

ARGONNE NATIONAL LABORATORY, ARGONNE, ILLINOIS

Operated by THE UNIVERSITY OF CHICAGO

for the U. S. DEPARTMENT OF ENERGY

under Contract W-31-109-Eng-38

Argonne National Laboratory, with facilities in the states of Illinois and Idaho, is owned by the United States government, and operated by The University of Chicago under the provisions of a contract with the Department of Energy.

DISCLAIMER

This report was prepared as an account of work sponsored by an agency of the United States Government. Neither the United States Government nor any agency thereof, nor any of their employees, makes any warranty, expressed or implied, or assumes any legal liability or responsibility for the accuracy, completeness, or usefulness of any information, apparatus, product, or process disclosed, or represents that its use would not infringe privately owned rights. Reference herein to any specific commercial product, process, or service by trade name, trademark, manufacturer, or otherwise, does not necessarily constitute or imply its endorsement, recommendation, or favoring by the United States Government or any agency thereof. The views and opinions of authors expressed herein do not necessarily state or reflect those of the United States Government or any agency thereof.

ANL/NDM-90

FAST-NEUTRON-SPECTRUM MEASUREMENTS FOR THE THICK-TARGET $^{9}Be(d,n)^{10}B$ REACTION AT E_d = 7 MeV*

by

D. L. Smith, J. W. Meadows and P. T. Guenther

April 1985

E NUCLEAR REACTION $^{9}Be(d,n)^{10}B$. Measured relative double-differential neutron-emission spectrum $\phi(E_n,\Theta)$, $0.8 \lesssim E_n < 12$ MeV and $0° < \Theta < 155°$, for 7-MeV deuterons on a thick Be target. Normalized data by comparison to results found in the literature. Examined some effects of anisotropic neutron emission on neutron-activation cross-section experiments.

Applied Physics Division
Argonne National Laboratory
9700 South Cass Avenue
Argonne, Illinois
USA

*This work supported by the U. S. Department of Energy.

NUCLEAR DATA AND MEASUREMENTS SERIES

The Nuclear Data and Measurements Series presents results of studies in the field of microscopic nuclear data. The primary objective is the dissemination of information in the comprehensive form required for nuclear technology applications. This Series is devoted to: a) measured microscopic nuclear parameters, b) experimental techniques and facilities employed in measurements, c) the analysis, correlation and interpretation of nuclear data, and d) the evaluation of nuclear data. Contributions to this Series are reviewed to assure technical competence and, unless otherwise stated, the contents can be formally referenced. This Series does not supplant formal journal publication but it does provide the more extensive information required for technological applications (e.g., tabulated numerical data) in a timely manner.

INFORMATION ABOUT OTHER ISSUES IN THE ANL/NDM SERIES:

A list of titles and authors for reports ANL/NDM-1 through ANL/NDM-50 can be obtained by referring to any report of this series numbered ANL/NDM-51 through ANL/NDM-76. Requests for a complete list of titles or for copies of previous reports should be directed to:

Section Secretary
Applied Nuclear Physics Section
Applied Physics Division
Building 316
Argonne National Laboratory
9700 South Cass Avenue
Argonne, Illinois 60439
USA

ANL/NDM-51 Measured and Evaluated Neutron Cross Sections of Elemental Bismuth by A. Smith, P. Guenther, D. Smith and J. Whalen, April 1980.

ANL/NDM-52 Neutron Total and Scattering Cross Sections of ^{6}Li in the Few MeV Region by P. Guenther, A. Smith and J. Whalen, February 1980.

ANL/NDM-53 Neutron Source Investigations in Support of the Cross Section Program at the Argonne Fast-Neutron Generator by James W. Meadows and Donald L. Smith, May 1980.

ANL/NDM-54 The Nonelastic-Scattering Cross Sections of Elemental Nickel by A. B. Smith, P. T. Guenther and J. F. Whalen, June 1980.

ANL/NDM-55 Thermal Neutron Calibration of a Tritium Extraction Facility using the ^{6}Li(n,t)^{4}He/^{197}Au(n,γ)^{198}Au Cross Section Ratio for Standardization by M. M. Bretscher and D. L. Smith, August 1980.

ANL/NDM-56 Fast-Neutron Interactions with ^{182}W, ^{184}W and ^{186}W by P. T. Guenther, A. B. Smith and J. F. Whalen, December 1980.

ANL/NDM-57 The Total, Elastic- and Inelastic-Scattering Fast-Neutron Cross Sections of Natural Chromium by Peter T. Guenther, Alan B. Smith and James F. Whalen, January 1981.

ANL/NDM-58 Review of Measurement Techniques for the Neutron Capture Process by W. P. Poenitz, August 1981.

ANL/NDM-59 Review of the Importance of the Neutron Capture Process in Fission Reactors by Wolfgang P. Poenitz, July 1981.

ANL/NDM-60 Gamma-Ray Detector Calibration Methods Utilized in the Argonne FNG Group Activation Cross Section Measurement Program by James W. Meadows and Donald L. Smith, April 1984

ANL/NDM-61 Fast-neutron Total and Scattering Cross Sections of ^{58}Ni by Carl Budtz-Jørgensen, Peter T. Guenther, Alan B. Smith and James F. Whalen, September 1981.

ANL/NDM-62 Covariance Matrices and Applications to the Field of Nuclear Data by Donald L. Smith, November 1981.

ANL/NDM-63 On Neutron Inelastic-Scattering Cross Sections of ^{232}Th, ^{233}U, ^{235}U, ^{238}U, ^{239}U, and ^{239}Pu and ^{240}Pu by Alan B. Smith and Peter T. Guenther, January 1982.

ANL/NDM-64 The Fission-Fragment Angular Distributions and Total Kinetic Energies for ^{235}U(n,f) from 0.18 to 8.83 MeV by James W. Meadows and Carl Budtz-Jørgensen, January 1982.

ANL/NDM-65 Note on the Elastic Scattering of Several-MeV Neutrons from Elemental Calcium by Alan B. Smith and Peter T. Guenther, March 1982.

ANL/NDM-66 Fast-neutron Scattering Cross Sections of Elemental Silver by Alan B. Smith and Peter T. Guenther, May 1982.

ANL/NDM-67 Non-evaluation Applications for Covariance Matrices by Donald L. Smith, July 1982.

ANL/NDM-68 Fast-neutron Total and Scattering Cross Sections of ^{103}Rh by Alan B. Smith, Peter T. Guenther and James F. Whalen, July 1982.

ANL/NDM-69 Fast-neutron Scattering Cross Sections of Elemental Zirconium by Alan B. Smith and Peter T. Guenther, December 1982.

ANL/NDM-70 Fast-neutron Total and Scattering Cross Sections of Niobium by Alan B. Smith, Peter T. Guenther and James F. Whalen, July 1982.

ANL/NDM-71 Fast-neutron Total and Scattering Cross Sections of Elemental Palladium by Alan B. Smith, Peter T. Guenther and James F. Whalen, June 1982.

ANL/NDM-72 Fast-neutron Scattering from Elemental Cadmium by Alan B. Smith and Peter T. Guenther, July 1982.

ANL/NDM-73 Fast-neutron Elastic-Scattering Cross Sections of Elemental Tin by C. Budtz-Jørgensen, Peter T. Guenther and Alan B. Smith, July 1982.

ANL/NDM-74 Evaluation of the ^{238}U Neutron Total Cross Section by Wolfgang Poenitz, Alan B. Smith and Robert Howerton, December 1982.

ANL/NDM-75 Neutron Total and Scattering Cross Sections of Elemental Antimony by A. B. Smith, P. T. Guenther and J. F. Whalen, September 1982.

ANL/NDM-76 Scattering of Fast-Neutrons from Elemental Molybdenum by Alan B. Smith and Peter T. Guenther, November 1982.

ANL/NDM-77 A Least-Squares Method for Deriving Reaction Differential Cross Section Information from Measurements Performed in Diverse Neutron Fields by Donald L. Smith, November 1982.

ANL/NDM-78 Fast-Neutron Total and Elastic-Scattering Cross Sections of Elemental Indium by A. B. Smith, P. T. Guenther, and J. F. Whalen, November 1982.

ANL/NDM-79 Few-MeV Neutrons Incident on Yttrium by C. Budtz-Jørgensen, P. Guenther, A. Smith and J. Whalen, June 1983.

ANL/NDM-80 Neutron Total Cross Section Measurements in the Energy Region from 47 keV to 20 MeV by W. P. Poenitz and J. F. Whalen, July 1983.

ANL/NDM-81 Covariances for Neutron Cross Sections Calculated Using a Regional Model Based on Elemental-Model Fits to Experimental Data by D. L. Smith and P. T. Guenther, November 1983.

ANL/NDM-82 Reaction Differential Cross Sections from the Least-Squares Unfolding of Ratio Data Measured in Diverse Neutron Fields by D. L. Smith, January 1984.

ANL/NDM-83 The Fission Cross Sections of Some Thorium, Uranium, Neptunium and Plutonium Isotopes Relative to ^{235}U by J. W. Meadows, October 1983.

ANL/NDM-84 ^{235}U and ^{239}Pu Sample-Mass Determinations and Intercomparisons by W. P. Poenitz and J. W. Meadows, November 1983.

ANL/NDM-85 Measurement of the $^{51}V(n,p)^{51}Ti$ Reaction Cross Section from Threshold to 9.3 MeV by the Activation Method by D. L. Smith, J. W. Meadows and I. Kanno, June 1984.

ANL/NDM-86 Energy-Differential Cross Section Measurement for the $^{51}V(n,\alpha)^{48}Sc$ Reaction by I. Kanno, J. W. Meadows, and D. L. Smith, July 1984.

ANL/NDM-87 Cross-Section Measurement for the $^{7}Li(n,n't)^{4}He$ Reaction at 14.74 MeV by D. L. Smith, J. W. Meadows, M. M. Bretscher and S. A. Cox, September 1984.

ANL/NDM-88 An Evaluated Nuclear Data File for Niobium by A. B. Smith, D. L. Smith and R. J. Howerton, March 1985.

ANL/NDM-89 Compilation and Evaluation of 14-MeV Neutron Activation Cross Sections for Nuclear Technology Applications: Set I by Bernard P. Evain, Donald L. Smith and Paul Lucchese, April 1985.

TABLE OF CONTENTS

	Page
Abstract	vii
I. Introduction	1
II. Experimental Procedure	2
III. Data Analysis	5
IV. Experimental Results and Errors	7
V. Some Effects of Anisotropic Neutron Emission	8
VI. Conclusions	10
Acknowledgements	10
References	11
Tables	14
Figures	23

FAST-NEUTRON-SPECTRUM MEASUREMENTS FOR THE THICK-TARGET $^{9}Be(d,n)^{10}B$ REACTION AT E_d = 7 MeV*

by

D. L. Smith, J. W. Meadows and P. T. Guenther

Applied Physics Division
Argonne National Laboratory
9700 South Cass Avenue
Argonne, Illinois 60439
USA

ABSTRACT

Spectra of neutrons with energies >800 keV which are emitted from a metallic beryllium target that is thick enough to completely stop 7-MeV incident deuterons are measured using organic scintillators and the pulse-beam time-of-flight method. Data are acquired for twenty different emission angles in the laboratory over the range 0-155 deg. The resulting information on the energy/angle detail of neutron emission is then employed in calculations which are performed in order to examine certain effects of the anisotropic neutron production on typical measurements of integral fast-neutron reaction cross sections.

*This work supported by the U.S. Department of Energy.

I. INTRODUCTION

For several years there has been considerable attention paid to various properties of the intense neutron sources provided by proton, deutron and alpha-particle bombardment of thick, light-element targets. The motivation for these studies arises from the various applications for these neutron sources in radiotherapy, radiation-damage research and neutron cross-section determination applications. The literature on this subject is too extensive to review here in its entirety, but the reader can capture the essential flavor of this area of endeavor from Refs. 1-7.

In the present work attention is focused specifically on the $^{9}Be(d,n)^{10}B$ reaction, and on its applications for neutron-induced reaction-cross-section data development and testing. The underlying concepts involved have been described in the literature, e.g., in Refs. 8-11. A very careful determination of the $^{9}Be(d,n)^{10}B$ thick-target spectrum at E_d = 7 MeV, for zero deg neutron-emission angle, has been made by Crametz et al. [12]. This particular neutron field has been reproduced at Argonne National Laboratory and used to obtain neutron-activation-reaction data for a number of elements. After analyzing these data closely, it was concluded that knowledge of the spectrum shape at zero deg alone is not sufficient to permit an accurate quantitative analysis and interpretation of these experimental results. For example, in order to perform neutron multiple-scattering calculations, and to deduce corrections for neutron absorption and non-uniform irradiation of samples which extend for several degrees beyond the zero-degree direction, it is necessary to have detailed information on the neutron spectrum away from zero deg. A search of the literature revealed that while some neutron-emission spectral data are available for laboratory angles other than zero deg, the existing data base is yet relatively sparse, and, in particular, no such information is available for E_d = 7 MeV. The objectives of the present investigation are thus: i) to measure the neutron-emission spectrum away from zero deg for the E_d = 7 MeV $^{9}Be(d,n)^{10}B$ source reaction, and ii) to examine some of the effects of anistropy on the analysis and interpretation of neutron-induced reation data measured in this neutron field under conditions commonly encountered in our laboratory.

Neutron emission from the $^{9}Be(d,n)^{10}B$ reaction is affected by the direct-reaction deuteron-stripping process. This process was first observed experimentally by Helmholz et al. [13], and the main features were explained theoretically by Serber [14] using a semi-empirical model. Subsequently, more sophisticated quantum-mechanical theories involving the Born Approximation, and more recently the Distorted-Wave Born Approximation (DWBA), have been proposed (e.g., see Refs. 15-16). The theory of Serber [14] continues to be used for predicting the general features of neutron emission, particularly for high-incident-deuteron-energy applications where so many nuclear levels, both bound and unbound, are involved that it is impractical to try to consider their individual properties. However, at lower energies, e.g., at the 7-MeV incident energy investigated in the present work, the detailed properties of individual levels are important and must be considered. In measurements

involving thin targets, e.g., certain of those performed by Weaver et al. [2], the effects of transitions leading to specific low-lying levels in ^{10}B can be seen in spectra acquired with resolutions adequate to distinguish these individual neutron groups. However, the main concern here is with the neutron yield from targets which are thick enough to stop the incident deuterons (~250μm for 7-MeV deuterons on beryllium metal [17]). Under these conditions, most of the detail corresponding to individual transitions is washed out. In general, one expects the neutron yield to be relatively forward-peaked for (d,n) reactions (e.g., see Refs. 15-16). However, the specific angular position of the maximum depends upon the angular momentum transfer for the reaction process. In $\ell = 0$ transitions, the peak yield is around zero deg. For transitions involving $\ell > 0$, the angular distribution maxima will generally occur at angles away from zero deg. According to the information compiled by Ajzenberg-Selove [18], the $^{9}Be(d,n)^{10}B$ transitions to individual levels in ^{10}B proceed via $\ell = 1$ for all of the levels below ~6 MeV excitation, except for the E_x = 4.77-MeV level ($\ell > 2$) and the E_x = 5.11 MeV level ($\ell = 0$). Thus, it is to be expected that the higher-energy portions of neutron-emission spectra from this reaction would tend toward maximum yields at emission angles other than zero deg. Since this had indeed been shown to be the case for E_d = 3.00, 8.84. 9.97, 10.97, 11.99, 14.05, 16.07, 18.09, 19.00 and 20.00 MeV by Weaver [1], there was no reason to believe that matters would be different at E_d = 7 MeV in the present investigation. The present concern, then, is simply a quantitative one.

The experimental procedure used in the present spectral measurements is described in Section II. The analysis of the measured data is discussed in Section III. Final results and errors are discussed in Section IV. Findings from certain calculations performed to test the impact of anisotropy in some typical nuclear-reaction cross section studies are presented in Section V. Finally, some conclusions from the present investigation are discussed in Section VI.

II. EXPERIMENTAL PROCEDURE

Pulsed-beam, time-of-flight spectroscopy (TOF) is the method used in the present experiment. The Argonne National Laboratory Fast-Neutron Generator (FNG) facility [19] was employed to produce pulsed and bunched deuteron beams with nominally ~2 nanosec time resolutions for gamma rays. A ten-angle TOF detector facility [20] was also used in this experiment because it provided both hardware and electronic components which could be easily adapted for the present investigation. However, only three of the ten available shielded-detector assemblies were actually active during this experiment. Detector No. 1 (D_1) was free to move between 0° and 155° in the laboratory, and it was used to acquire all the primary spectral data. Detectors No. 5 (D_5) and No. 8 (D_8) were placed at 61.5° and 107.5°, respectively. They were used to record secondary spectra for relative neutron fluence monitoring purposes.

All inactive detector assemblies were left in close proximity to the monitors D_5 and D_8, thereby enhancing the shielding. The deuteron beam from the FNG accelerator was directed to a special low-mass beryllium target assembly, designed and constructed explicitly for this experiment. It was situated at the center of rotation of the detector array so that it could be viewed without obstruction by each active detector. This experimental setup is shown schematically in Fig. 1.

The beryllium target apparatus is shown schematically in Fig. 2. It has a low-mass design so as to minimize neutron absorption and scattering. The side walls of the assembly are 0.05-cm-thick stainless steel. The end caps where the beryllium target wafers are situated are also 0.05-cm-thick and they are made either of stainless steel or tantalum. The flanges are fabricated of somewhat thicker stock, but no detector viewed any of these flanges. It is estimated that an upper limit for the net neutron scattering and absorption effects is <3%. The relative variation from one angle to another is smaller, so no attempt was made to correct the data for target perturbations. Most measurements were performed with the beryllium target wafer situated perpendicular to the incident deuteron beam (Be 90). Use was made in measurements near 90° of a special target cap which places a beryllium wafer at 45° to the deuteron beam (Be 45), thus avoiding possibly-significant neutron spectrum perturbation by the target. The beryllium target wafers were 0.05-cm thick disks (more than thick enough to stop 7-MeV deuterons). Other target caps containing tantalum beam stops were employed for background measurements. The deuteron beam on target had to be reduced to quite a low level for this experiment (discussed below). This was accomplished by means of a tantaluum aperture. Insulator rings were employed so that the target and aperture currents could be monitored independently.

Only one detector was used to measure the primary $^9Be(d,n)^{10}B$ spectra in order to avoid the difficulty of having to accurately intercalibrate ten separate detectors for measurements over the wide neutron-energy range (0.8 - 12 MeV) required for this experiment. This detector was a 2.54-cm-diam by 0.635-cm-thick NE-102A plastic scintillator button (no gamma-ray discrimination was possible). The distance from the beryllium target to the center of the scintillator was measured to be 503.2 ± 0.2 cm. This distance varied by <0.2 cm over the angular range 0-155°. The two monitor detectors were 12.7 cm diam x 2.0-cm-thick NE-213 liquid scintillators. Gamma-ray discrimination circuitry for these channels permitted a rather substantial degree of suppression of the gamma-ray events recorded by the monitors. The monitor detectors were also situated ~5 m from the beryllium target. Since the efficiencies of the monitor detectors far exceeded that of the primary detector, it proved worthwhile to reduce the fluence incident upon them by plugging the monitor-detector collimators (D_5 and D_8 in Fig. 1) with ~15-cm-thick lucite plugs. While this distorted the spectra seen by the monitors, it did not affect their usefulness for relative target-neutron fluence determination from run to run.

The experimental data were recorded using an on-line computer. In this experiment it was not intended to measure absolute neutron spectra, but only relative spectra from angle to angle. It was decided to rely upon the absolutely-normalized results of Crametz et al. [12] at zero deg to provide the overall normalization. All the present measurements were yield determinations relative to zero deg. Since the primary-detector data and monitor data were

simultaneously recorded, computer deadtime effects cancelled. The monitor-detector environments were largely independent of the angular position of the primary detector. Thus, there were really only two possible considerations concerning normalization of the data: i) stability of the individual detectors, and ii) variation of the efficiency within any one detector due to count-rate-dependent deadtime of its corresponding analog circuitry. Since the geometries of the monitor detectors were fixed for all measurements, it was easy to trace their stability by examining the ratio of the yields, or by consideration of the ratio of individual monitor detector yields to the recorded integrated target and aperture deuteron beam currents from run to run. For the mobile primary detector reliance was placed on repetition of measurements at various angles, especially at zero deg, to determine the stability of the effective intrinsic detector efficiency.

It was learned early in this investigation that the neutron yield from a thick beryllium target for typical FNG pulsed-beams (~1-5 μA average current) was much too large to allow the intended experiment to be performed. Thus, various measurements were made to determine acceptable beam conditions. Target currents had to be low enough so that deadtimes in the analog circuitry for all of the individual detector channels were acceptably small. At the same time, the beam intensity at the beam pickoff loop had to be large enough to yield a reliable timing signal. Ultimately, by carefully adjusting the operating parameters of the FNG and the beam-defining slit opening, it was possible to obtain satisfactory results using a target aperture of 0.08 cm diam, with beam currents ~0.015-0.060 μA on target and ~0.050-0.160 μA on the aperture. The aperture was kept clean, and all the other beam-defining slits near the target were opened in order to minimize the effects of background neutrons from extraneous sources other than the beryllium target itself.

Calibration of the deuteron-beam energy was based upon magnetic analysis and threshold measurements for the $^{7}Li(p,n)^{7}Be$ and $^{11}B(p,n)^{11}C$ reactions [21]. These measurements were made on another beam line which contains precision magnetic beam analysis apparatus. The stability of the beam energy on target for the beam line actually used to acquire the present data was monitored by measuring the accelerator terminal potential. The uncertainty in this process was the main source of error in controlling the beam energy. Overall it was concluded that the deuteron-beam energy remained in the range 7.00 ± 0.03 MeV for the entire experiment.

An accurate frequency meter and a series of delay cables were used to deduce the time-per-channel calibration for the recorded spectra. A prompt gamma-ray peak was present in all spectra (even in the monitor spectra since gamma-ray suppression was not complete). These peaks provided convenient calibration points for use in determination of the neutron-energy scale. A second useful calibration mark was obtained by observing the resonance absorption dip at 2078.1 ± 0.3 keV in carbon [22]. This was observed for all spectra from the monitor detectors (D_5 and D_8) since the lucite plugs contain carbon. For the primary detector (D_1), the 2078.1-keV resonance dip was observed periodically using a 4-cm-thick graphite block placed in front of the collimator. These measurements established the energy scale and monitored the stability of the TOF system.

Production runs were typically of 30-60 minutes in duration. Spectral data were taken at the following laboratory angles for D_1: 0°, 2.5°, 5°, 7.5°, 10°, 15°, 20°, 30°, 45°, 53°, 68°, 75°, 83°, 90°, 100°, 110°, 120°, 130°, 141° and 155°. These angles were determined to better than 0.5° on an absolute basis. Measurements were performed more than once for most of these angles, and background spectra were obtained using tantalum targets over the entire angular range. Comparisons were made between the spectra recorded using the two different beryllium target caps, Be 90 and Be 45, at 0°, 75°, 90° and 110°. The differences were negligible at 0°, 75° and 110°. At 90°, the target Be 90 yielded fewer events (< 10% difference) per unit of neutron fluence than did Be 45. The possibility for substantial absorption loss from target Be 90 near the 90°-emission angle is inherent to the basic design (see Fig. 2).

Based on the prompt gamma-ray peaks, the overall timing resolution was $\lesssim$2 nanosec for gamma rays. From an observation of monoenergetic $^7Li(p,n)^7Be$ neutrons, it was concluded that there was relatively little collimator in-scattering of the neutrons, but that the timing resolution for neutron detection was somewhat worse than for gamma rays, with resolutions ~3 nanosec quite typical.

III. DATA ANALYSIS

Analysis of the measured TOF spectra involved the following essential steps: i) determination of the energy scale, ii) removal of background, iii) relative normalization of the accumulated results, iv) conversion from time spectra to energy spectra, and v) adjustment for detector efficiency and absolute normalization of all the data based on the results of Crametz et al. [12] at zero deg. At each stage of the analysis, data tests were performed in order to check on the stability of the individual detector efficiency calibrations and on the TOF calibration.

The locations of the prompt gamma-ray peaks and 2078.1-keV carbon resonance dips (where applicable) were deduced using computer algorithms. These positions were stable throughout the experiment to within ~1-2 channels. Since the time calibration for this experiment was 0.993 ± 0.003 nanosec/ch for all spectra, this stability of the TOF calibration exceeded the resolution of the measurements. The neutron energy scale for this experiment was derived from the measured flight path, time-per-channel and position of the prompt gamma-ray peak in each spectrum. Non-relativistic analysis was used since relativistic effects were found to amount to <0.2 nanosec (~50 keV at 12-MeV neutron energy), an amount far smaller than the time resolution of the experiment. Energy calibration check points were the 2078.1-keV carbon resonance dip, the sharp discontinuity in the zero-degree neutron spectrum at ~6.2 MeV, and the endpoint of the spectrum [12]. Since the Q-value for the $^9Be(d,n)^{10}B$ reaction is 4.361 MeV [23], the endpoint at zero deg is ~11.4 MeV. The energy-scale calibration derived for this experiement was consistent with these three check points within the experimental resolution.

The available tantalum-target data were normalized to the corresponding beryllium-target data using the integrated target currents for each run. The ratio of target to aperture current was consistent to within ~20% for most of the runs, and the relative yield of all background events to all $^{9}Be(d,n)^{10}B$ events was relatively small. For detector D_1, they amounted to ~0.2-4%, depending on angle, as shown in Fig. 3. After subtracting the background, as deduced from the tantalum target data, it was observed that a relatively small and apparently time-uncorrelated, residual background was still present in each spectrum. The magnitude of this background was estimated by averaging the content of several channels in regions of the spectra which were clearly devoid of direct $^{9}Be(d,n)^{10}B$ neutron events. These backgrounds were then subtracted from the TOF spectra. The final corrected spectra were uniformly "clean" in appearance, indicating that the remaining events were essentially all due to unscattered neutrons from $^{9}Be(d,n)^{10}B$. Based on the energy calibration discussed above, it was concluded that the energy cutoff point in the primary detector D_1 was ~800 keV for most of the recorded data.

All spectra were summed over the regions of significant fast-neutron yield in order to test the experimental data for consistency. The ratios of events in the monitor detectors D_5 and D_8 varied by $\lesssim$ 1%, indicating that these detectors were very stable over the course of the experiment. It was decided to employ the sum of the background-corrected fast-neutron yields from these detectors as the parameter for relative normalization of the primary detector D_1 data. Ratios of the total yield of D_1 to this monitor parameter were calculated and plotted versus the laboratory angle of D_1. This provided two important pieces of information: i) early in the course of the experiment there occured a sudden significant change in the efficiency of D_1 (between two runs), and ii) other than this single anomalous experimental event, the stability of detector D_1 was very good, as indicated by the smooth variation and reproducibility of the raw-event yield versus angle. Fortunately, the two sets of data, separated by the anomalous efficiency shift mentioned above, each included one or more zero-deg beryllium-target runs. Therefore, these two sets could be analyzed independently of each other. Ratios of the summed raw counts for detectors D_5 and D_8 to the integrated target currents were generally consistent to within ±5%, thus indicating that the overall deadtime for the electronics system was not very large. This is consistent with the fact that the count rates for processed fast-neutron events were not excessive: detector D_1 (< 400 cps), detector D_5 (< 130 cps), and detector D_8 (< 80 cps).

Corrected detector D_1 TOF spectra, normalized as described above were next converted to energy-group form by summing events in selected groups of adjacent channels and dividing these sums by the corresponding energy interval represented in the sum. The choice of group limits was dictated by two considerations: i) each group was to represent no less than ~200-keV width, and ii) each group had to include no fewer than three TOF-spectrum channels (consistent with the experimental resolution). The first group (~800-1000 keV) included 44 channels, while all groups above ~5.2 MeV consisted of exactly 3 channels. The energy group structure is given in Table 1. Two major steps remained to be discussed for the data analysis procedure:

i) adjustment of the energy-group spectra for the neutron-energy-dependent efficiency of detector D_1, and ii) absolute normalization of all spectra. The required analysis is discussed in the following paragraph.

An efficiency curve for detector D_1 was not directly determined. Instead, an effective efficiency curve was deduced by dividing the present zero-deg spectra by the spectrum reported by Crametz et al. [12], after converting the latter to dimensions of $n.sr^{-1}.keV^{-1}.\mu C^{-1}$ and casting it into a group format consistent with the present experiment. The resulting efficiency curve was very reasonable in shape. Smooth eyeguides were drawn through the extracted efficiency values in order to avoid the effects of a few anomalous points (especially ~6.2 MeV where the $^9Be(d,n)^{10}B$ spectrum exhibits a sharp discontinuity with energy at zero deg). The reasonableness of the shape of the derived efficiency curve was confirmed by calculations performed with code CARLO-BLACK [24]. These calculations were based on the known geometry of detector D_1 and the observed neutron cutoff in the TOF spectra. A comparison of the calculated and experimentally-derived shapes is shown in Fig.4.

IV. EXPERIMENTAL RESULTS AND ERRORS

The final results of the present experiment are listed in Table 1 and are also plotted in Fig. 5. Although more than one measurement was made at each angle, corresponding spectra were found to be very similar for all the angles and were thus merged to provide a single spectrum per angle, with corresponding reduction of the random error.

The manner of presentation of data in Table 1 and Fig. 5 provides little insight into the angular distribution properties of the emitted neutrons. In order to shed light on this facet of the experimental results, sums were made over contiguous energy ranges of ~2-MeV width for each of the spectra, and the results are plotted in Fig. 6 vs. laboratory emission angle. Also, the total neutron yield above ~800 keV is plotted vs. angle in that figure. The total neutron yield above ~800 keV is clearly forward-peaked, as is that for each of the indicated energy bands below ~6.9 MeV, excluding a small dip in the yield near zero deg. However, the yield above ~6.9 MeV is clearly not forward-peaked, and strong evidence is seen for $\ell>0$ stripping processes, as discussed in Section I.

The experimental errors for the results given in Table 1 involve several components of both a random and systematic nature. The errors in the recorded spectral counts were carefully propagated through the entire data analysis process, from recorded TOF spectra to final energy-group results, using methods described in Ref. 25. These errors are given explicitly in Table 1, and they range from 0.3% to 95.8%, with the errors for most groups being smaller than 5%. The smallest errors are found in the lower energy-group regions and the largest ones near the high-energy end points of the spectra. These errors are mostly uncorrelated from group to group and can be treated as random. Because

of the rather involved approach used to deduce the effective efficiency for the primary detector D_1 in this experiment, there are several related systematic error sources to be considered. First, there is uncertainty in the process of comparing the zero-deg results from the present experiment with the spectrum of Crametz et al. [12]. Recall from Section III that this involved casting the spectrum of Crametz et al. [12] into the present energy-group format, dividing corresponding spectra, and then sketching eyeguides through the resulting values. It is estimated that the uncertainty in this procedure is: $E_n < 1.5$ MeV (5%), $1.5 < E_n < 3.8$ MeV (2%), $3.8 < E_n < 5.7$ MeV (3%), $5.7 < E_n < 8$ MeV (4%), $8 < E_n < 10.5$ MeV (5%), and $E_n > 10.5$ MeV (7%). The correlation between the errors in adjacent energy regions is thought to be $\lesssim 50\%$, while it is probably negligible for non-adjacent regions. For applications in which the present results are to be used in an absolutely-normalized sense, the uncertainties in the zero-deg results of Crametz et al. [12] must be added. These uncertainties are discussed at length in Refs. 12 and 26, so the details will not be repeated here. The main elements of this uncertainty are: overall normalization (3-4%), relative uncertainty in the spectrum shape due to detector calibration (2-5%), and statistical errors (1-9%). Note, however, that the uncertainties in the reference spectrum of Crametz et al. [12] need not be considered in a number of applications where the relative yields from energy group to energy group and angle to angle are required for the analysis of corrections, e.g., as described in Section V. Neutron scattering and absorption not only add and remove events from the spectra, but they also lead to energy redistribution. As discussed in Section II, the present experimental apparatus was designed to be of low mass so that the effect could be neglected. It is difficult to calculate rigorously. The effect is conservatively estimated as being smaller than 3%, so an error of 3% is assumed. There are likely to be strong correlations between the errors in adjacent energy groups and for adjacent angles, but no attempt was made to estimate them. The uncertainty involved in normalizing the various experimental runs to each other by means of the monitor data appears to be ~1% and it is random. No attempt was made to estimate errors which could be attributed to uncertainties in the experimental angles or in the deuteron- and neutron-energy scales.

V. SOME EFFECTS OF ANISOTROPIC NEUTRON EMISSION

The effects of anisotropic emission of neutrons from a near-point source, such as the one under present consideration, depend upon the application in question. To illustrate some possibilities, this section presents examples in which the impact upon the measurement of activation cross sections is treated. The experiment envisioned is that in which two reactions, an unknown reaction and a monitor reaction, are involved. The measured quantity is a ratio, though ultimately one seeks an integral cross section for the unknown reaction in the 7-MeV $^9Be(d,n)^{10}B$ thick-target neutron field, is based upon calculations involving the monitor-reaction cross section which is presumed to be known.

The experimental geometry involves two sample disks which occupy nearly the same spatial position perpendicular to the incident-deuteron beam line (zero-deg neutron emission angle). Corrections to the measured ratio data are required for two reasons: i) the samples have a finite extent, with sample material intercepting target neutrons over the angular range zero to Θ_{max} (i.e., total angle subtended by the sample is $2\Theta_{max}$), and ii) neutrons scattered from the target structures can affect the measured cross-section ratio.

First, consider the "finite" geometry effect. Simulated cross-section calculations were performed using the neutron-emission data from Table 1, for the reactions $^{58}Ni(n,p)^{58}Co$, $^{27}Al(n,p)^{27}Mg$, $^{63}Cu(n,\alpha)^{60}Co$, $^{60}Ni(n,p)^{60}Co$ and $^{27}Al(n,\alpha)^{24}Na$, and for a hypothetical "flat" (no energy dependence) cross section, relative to the fast-neutron fission of ^{238}U. ENDF/B-V [27] evaluated cross sections were used for all the reactions except for $^{63}Cu(n,\alpha)^{60}Co$, which was derived instead from the work of Winkler et al. [28]. Comparison was made between the calculated results obtained using the presently-measured neutron-emission data and those obtained assuming isotropic neutron emission. Several geometries were considered, as summarized in Table 2. It is seen that the effects of anisotropic neutron emission can be very substantial for typical experimental geometries, with the greatest impact on the ratios occuring when the reaction thresholds involved are substantially different.

A very practical and specific application of the data provided by the present investigation involves a re-examination of the experiment of Liskien et al. [10]. In this experiment, a 2-cm-diam x 0.5 cm-thick Al-Cu alloy sample was irradiated at a distance of 8 cm from the E_d = 7 MeV $^{9}Be(d,n)^{10}B$ thick-target neutron source in order to measure the integral ratio of $^{63}Cu(n,\alpha)^{60}Co$-to-$^{27}Al(n,\alpha)^{24}Na$. These investigators obtained the value 0.539 ± 0.009 for this ratio. No correction for anistropic neutron emission was applied in their analysis. In this experiment $\Theta_{max} \approx 7.1°$ (i.e., ~14° subtended), and it has been determined as a result of the present work that their reported value should be increased by ~9.4% to account for neutron anistropy. When this is done, the corrected value of 0.589 is in excellent agreement with the calculated value of 0.587 reported in their paper.

In practice, a target assembly with mass as low as that indicated in Fig. 2 cannot be used in typical activation experiments because it could not adequately dissipate the beam power (which typically approaches 100 watt). Consequently, neutron scattering from more massive beryllium target assemblies is a practical concern for such neutron activation experiments. To investigate this effect, the neutron scattering from a beryllium target imbedded in a copper beam stop, 7.0-cm in diam x 0.2-cm thick with a 2.0-cm-diam recess to 0.05-cm thickness in the vicinity of the beam spot, was investigated using Monte-Carlo calculations. The above-mentioned reactions were considered and the results given in Table 3 were obtained. As shown in Fig. 6, the $^{9}Be(d,n)^{10}B$ thick-target reaction at E_d = 7 MeV is generally forward-peaked, and this often leads to a substantial (and fortunate) reduction in the required scattering corrections, relative to the corresponding situation for isotropic emission.

VI. CONCLUSIONS

The results of the present experiment indicate that the neutron emission from the 7-MeV $^{9}Be(d,n)^{10}B$ thick-target reaction is indeed quite anisotropic. The observed anisotropy is consistent with the data of Weaver et al. [1,2] at both higher and lower deuteron energies. Although the neutron emission tends to be forward-peaked, the higher-energy portion of the spectrum (>6.9 MeV) is strongly influenced by $\ell>0$ (d,n)-stripping and thus does not peak at zero deg.

The effect of this anisotropy on integral-reaction cross-section measurements can be substantial whenever the irradiated samples subtend significant solid angles relative to the source. Corrections can (and should) be applied under such circumstances. On the other hand, the generally-forward peaked nature of the neutron emission suggests that the effects of neutron scattering by target structures can be minimized by appropriate design.

ACKNOWLEDGEMENTS

The authors are indebted to A. B. Smith for permitting the use of his ten-channel neutron-scattering apparatus. This work was supported by the U.S. Department of Energy.

REFERENCES

1. K. A. Weaver, "Neutrons from Deuteron Bombardment of Light Nuclei", UCRL-51310, Lawrence Livermore Laboratory (1972); see also K. A. Weaver, "Spectra of Neutrons from Deuteron Bombardment of Light Nuclei", UCLR-51310-Addendum, Lawrence Livermore Laboratory (1973).

2. K. A. Weaver, J. D. Anderson, H. H. Barschall, and J. C. Davis, Nuclear Science and Engineering 52, 35 (1973).

3. P. Grand and A. N. Goland, Nuclear Instruments and Methods 145 (1977) 49.

4. M. J. Saltmarsh, C. A. Ludemann, C. B. Fulmer, and R. C. Styles, Nuclear Instruments and Methods 145 (1977) 81.

5. D. W. Kneff, Harry Farrar IV, L. R. Greenwood, and M. W. Guinan, "Characterization of the Be(d,n) Neutron Field By Passive Dosimetry Techniques", Proceedings of a Symposium on Neutron Cross Sections from 10 to 50 MeV, Brookhaven National Laboratory, Upton, New York, May 12-14, 1980, BNL-NCS-51245 (Vol. I), edited by M. R. Bhat and S. Pearlstein, Brookhaven National Laboratory, July 1980, p. 113.

6. M. A. Lone and B. C. Robertson, "Low Energy Neutron Emission From Be(d,n) and Be(p,n) Reactions", Proceedings of a Symposium on Neutron Cross Sections from 10 to 50 MeV, Brookhaven National Laboratory, Upton, New York, May 12-14, 1980, BNL-NCS-51245 (Vol. I) edited by M. R. Bhat and S. Pearlstein, Brookhaven National Laboratory, July 1980, p. 147.

7. M. A. Lone and C. B. Bigham, "Intense Deuteron and Proton Induced (CW)-Neutron Sources", Neutron Sources for Basic Physics and Applications, edited by S. Cierjacks, Pergamon Press, Oxford, United Kingdom (1983) p. 133.

8. L. R. Greenwood, R. R. Heinrich, R. J. Kennerly, and R. Medrzychowski, Nuclear Technology 41, 109 (1978).

9. L. R. Greenwood and R. R. Heinrich, Journal of Nuclear Materials 85 and 86 (1979) 473.

10. H. Liskien, D. L. Smith, and R. Widera, "The Spectrum-Average Cross Section Ratio of $^{63}Cu(n,\alpha)^{60}Co$-to-$^{27}Al(n,\alpha)^{24}Na$ in a Thick-Target $^{9}Be(d,n)^{10}B$ Neutron Spectrum", Nuclear Data for Science and Technology, edited by K. H. Böckhoff, D. Reidel Publishing Company, Dordrecht, Holland (1983), p. 409.

11. Donald L. Smith, "A Least-Squares Method for Deriving Reaction Differential Cross Section Information from Measurements in Diverse Neutron Fields", ANL/NDM-77, Argonne National Laboratory (1982).

12. A. Crametz, H. -H. Knitter, and D. L. Smith, "Thick-Target $^{9}Be(d,n)^{10}B$ Neutron Spectrum at E_d = 7 MeV", Nuclear Data for Science and Technology, edited by K. H. Böckhoff, D. Reidel Publishing Company, Dordrecht, Holland (1983), p. 902.

13. A. C. Helmholz, E. M. McMillan, and D. C. Sewell, Physical Review 72 (1947) 1003.

14. R. Serber, Physical Review 72 (1947) 1008.

15. S. T. Butler, Nuclear Stripping Reactions, John Wiley and Sons, Inc., New York (1957).

16. W. Tobocman, Theory of Direct Nuclear Reactions, Oxford University Press, London, United Kingdom (1961).

17. H. H. Anderson and J. F. Ziegler, Hydrogen Stoping Powers and Ranges in All Elements, Pergamon Press, New York (1977).

18. F. Ajzenberg-Selove, Nuclear Physics A413 (1984) 1.

19. S. A. Cox and P. R. Hanley, IEEE Transactions on Nuclear Science 18, 108 (1971).

20. A. Smith, P. Guenther, R. Larson, C. Nelson, P. Walker, and J. Whalen, Nuclear Instruments and Methods 50, 277 (1967).

21. E. H. Beckner, R. L. Bramblett, G. C. Phillips, and T. A. Eastwood, Physical Review 123, 2100 (1961).

22. S. F. Mughabghab, M. Divadeenam, and N. E. Holden, Neutron Cross Sections (Vol. 1): Neutron Resonance Parameters and Thermal Cross Sections, Part A, Z = 1-60, Academic Press, New York (1981).

23. C. Michael Lederer and Virginia S. Shirley, Table of the Isotopes, 7th Edition, John Wiley and Sons, Inc., New York (1978).

24. W. P. Poenitz, "The Black Neutron Detector", ANL-7915, Argonne National Laboratory, Argonne, Illinois (1972).

25. Donald L. Smith, "Covariance Matrices and Applications to the Field of Nuclear Data", ANL/NDM-62, Argonne National Laboratory (1981).

26. D. L. Smith and H. Liskien, "Error Analysis for the Calculated Spectrum-Average Cross Section Ratio of $^{63}Cu(n,\alpha)^{60}Co$-to-$^{27}Al(n,\alpha)^{24}Na$ in a Thick-Target $^{9}Be(d,n)^{10}B$ Spectrum", European Applied Research Reports, Vol. 4, No. 4, 969-1012 (1982).

27. "Evaluated Neutron Data File, ENDF/B-V", ENDF/B Summary Documentation, compiled by R. Kinsey, ENDF-201, 3rd Edition, Brookhaven National Laboratory (1979).

28. G. Winkler, D. L. Smith, and J. W. Meadows, "On the Discrepancy Between Differential and Integral Results for the $^{63}Cu(n,\alpha)^{60}Co$ Cross Section", Proceedings of the International Conference on Nuclear Cross Sections for Technology, Knoxville, Tennessee, October 22-26, 1979, published as Nuclear Cross Sections for Technology, NBS Special Publication 594, eds. J. L. Fowler, C. H. Johnson, and C. D. Bowman, National Bureau of Standards, U.S. Dept. of Commerce, Washington, D.C., p. 199 (1980).

Table 1: Measured Neutron-Emission Spectra for the $^{9}Be(d,n)^{10}B$ Thick-Target Reaction at E_d = 7 MeV

Neutron Flux in neutrons/(sr . keV . microC) with Random Error in %

Group	Energy Range (keV)		0 deg		2.5 deg		5 deg	
1	798.1	1002.0	0.77318E+06	.6	0.80336E+06	1.2	0.75013E+06	.8
2	1002.0	1203.7	0.81885E+06	.4	0.86695E+06	.8	0.83658E+06	.6
3	1203.7	1416.0	0.84374E+06	.4	0.85916E+06	.7	0.83958E+06	.5
4	1416.0	1620.0	0.88449E+06	.3	0.90054E+06	.7	0.87026E+06	.5
5	1620.0	1816.7	0.91972E+06	.3	0.93221E+06	.6	0.90728E+06	.4
6	1816.7	2019.8	0.96170E+06	.3	0.99107E+06	.6	0.95139E+06	.4
7	2019.8	2222.2	0.97299E+06	.3	0.10033E+07	.6	0.96073E+06	.4
8	2222.2	2435.8	0.97484E+06	.3	0.99925E+06	.5	0.95626E+06	.4
9	2435.8	2634.3	0.97061E+06	.3	0.99516E+06	.6	0.94890E+06	.4
10	2634.3	2831.8	0.95412E+06	.3	0.97431E+06	.6	0.93670E+06	.4
11	2831.8	3052.5	0.93206E+06	.3	0.95364E+06	.5	0.91967E+06	.4
12	3052.5	3267.4	0.90988E+06	.3	0.92443E+06	.5	0.88568E+06	.4
13	3267.4	3470.2	0.86581E+06	.3	0.89996E+06	.6	0.85021E+06	.4
14	3470.2	3692.4	0.80236E+06	.3	0.81958E+06	.6	0.80314E+06	.4
15	3692.4	3894.4	0.77092E+06	.3	0.78718E+06	.6	0.75550E+06	.4
16	3894.4	4113.4	0.75917E+06	.3	0.76051E+06	.6	0.73893E+06	.4
17	4113.4	4302.2	0.71984E+06	.4	0.73693E+06	.7	0.71337E+06	.5
18	4302.2	4504.3	0.69195E+06	.4	0.71041E+06	.7	0.67894E+06	.5
19	4504.3	4720.9	0.66180E+06	.4	0.68218E+06	.7	0.64764E+06	.5
20	4720.9	4953.6	0.64033E+06	.4	0.65035E+06	.7	0.62236E+06	.5
21	4953.6	5203.9	0.62828E+06	.4	0.64145E+06	.7	0.60761E+06	.5
22	5203.9	5404.3	0.55084E+06	.4	0.55644E+06	.8	0.53858E+06	.6
23	5404.3	5616.6	0.49016E+06	.5	0.49422E+06	.8	0.47033E+06	.6
24	5616.6	5841.5	0.48736E+06	.4	0.49802E+06	.8	0.46319E+06	.6
25	5841.5	6080.3	0.45710E+06	.5	0.47022E+06	.8	0.43398E+06	.6
26	6080.3	6333.9	0.25505E+06	.6	0.25591E+06	1.1	0.28316E+06	.7
27	6333.9	6603.8	0.94012E+05	1.0	0.10771E+06	1.7	0.11838E+06	1.1
28	6603.8	6891.4	0.81425E+05	1.1	0.85562E+05	1.9	0.89603E+05	1.3
29	6891.4	7198.1	0.82256E+05	1.0	0.83261E+05	1.9	0.90266E+05	1.2
30	7198.1	7525.8	0.85455E+05	1.0	0.87601E+05	1.8	0.93121E+05	1.2
31	7525.8	7876.3	0.85437E+05	1.0	0.87771E+05	1.7	0.97520E+05	1.1
32	7876.3	8252.0	0.76918E+05	1.0	0.82236E+05	1.7	0.91491E+05	1.1
33	8252.0	8655.1	0.80319E+05	.9	0.85615E+05	1.6	0.93376E+05	1.1
34	8655.1	9088.6	0.76524E+05	.9	0.85727E+05	1.6	0.94227E+05	1.0
35	9088.6	9555.4	0.66220E+05	1.0	0.75371E+05	1.6	0.87212E+05	1.1
36	9555.4	10059.2	0.47756E+05	1.1	0.53076E+05	1.9	0.68439E+05	1.2
37	10059.2	10603.8	0.38723E+05	1.2	0.45899E+05	2.0	0.54934E+05	1.3
38	10603.8	11194.0	0.26382E+05	1.4	0.31664E+05	2.3	0.40257E+05	1.4
39	11194.0	11834.8	0.88668E+04	2.6	0.10943E+05	4.0	0.17510E+05	2.1

Neutron Flux in neutrons/(sr . keV . microC) with Random Error in %

Group	Energy Range (keV)		7.5 deg		10 deg		15 deg	
1	798.1	1002.0	0.71551E+06	1.2	0.72698E+06	.8	0.67538E+06	.9
2	1002.0	1203.7	0.80095E+06	.8	0.77476E+06	.5	0.73530E+06	.6
3	1203.7	1416.0	0.82308E+06	.7	0.78191E+06	.5	0.72098E+06	.5
4	1416.0	1620.0	0.84175E+06	.7	0.80921E+06	.4	0.72527E+06	.5
5	1620.0	1816.7	0.87462E+06	.6	0.82608E+06	.4	0.73392E+06	.5
6	1816.7	2019.8	0.92680E+06	.6	0.85058E+06	.4	0.76385E+06	.5
7	2019.8	2222.2	0.94013E+06	.6	0.85838E+06	.4	0.74787E+06	.5
8	2222.2	2435.8	0.92358E+06	.5	0.84883E+06	.4	0.73557E+06	.4
9	2435.8	2634.3	0.91739E+06	.6	0.84193E+06	.4	0.72256E+06	.4
10	2634.3	2831.8	0.90437E+06	.6	0.81791E+06	.4	0.69891E+06	.5
11	2831.8	3052.5	0.88063E+06	.5	0.79288E+06	.4	0.67161E+06	.4
12	3052.5	3267.4	0.84535E+06	.5	0.76601E+06	.4	0.63991E+06	.4
13	3267.4	3470.2	0.80521E+06	.6	0.72724E+06	.4	0.60611E+06	.5
14	3470.2	3692.4	0.74238E+06	.6	0.68201E+06	.4	0.55541E+06	.5
15	3692.4	3894.4	0.71485E+06	.6	0.64595E+06	.5	0.53763E+06	.5
16	3894.4	4113.4	0.69835E+06	.6	0.63954E+06	.4	0.52528E+06	.5
17	4113.4	4302.2	0.66717E+06	.7	0.60926E+06	.5	0.50184E+06	.6
18	4302.2	4504.3	0.63955E+06	.7	0.58056E+06	.5	0.48248E+06	.6
19	4504.3	4720.9	0.60607E+06	.7	0.55061E+06	.5	0.44699E+06	.6
20	4720.9	4953.6	0.59056E+06	.7	0.53334E+06	.5	0.42420E+06	.6
21	4953.6	5203.9	0.55222E+06	.7	0.51412E+06	.5	0.39165E+06	.6
22	5203.9	5404.3	0.45595E+06	.8	0.43491E+06	.6	0.31418E+06	.7
23	5404.3	5616.6	0.42600E+06	.8	0.36467E+06	.6	0.27652E+06	.8
24	5616.6	5841.5	0.42508E+06	.8	0.36698E+06	.6	0.27259E+06	.7
25	5841.5	6080.3	0.38139E+06	.9	0.35345E+06	.6	0.25397E+06	.8
26	6080.3	6333.9	0.17643E+06	1.3	0.23361E+06	.8	0.16221E+06	.9
27	6333.9	6603.8	0.10400E+06	1.6	0.11391E+06	1.1	0.12136E+06	1.1
28	6603.8	6891.4	0.93671E+05	1.7	0.10029E+06	1.2	0.11683E+06	1.1
29	6891.4	7198.1	0.99201E+05	1.6	0.10433E+06	1.1	0.12363E+06	1.0
30	7198.1	7525.8	0.10903E+06	1.5	0.11089E+06	1.0	0.13605E+06	.9
31	7525.8	7876.3	0.11056E+06	1.4	0.11688E+06	1.0	0.14553E+06	.9
32	7876.3	8252.0	0.10862E+06	1.4	0.11427E+06	1.0	0.15134E+06	.9
33	8252.0	8655.1	0.11579E+06	1.3	0.12260E+06	.9	0.16507E+06	.8
34	8655.1	9088.6	0.11744E+06	1.3	0.12902E+06	.9	0.17269E+06	.8
35	9088.6	9555.4	0.10269E+06	1.4	0.12370E+06	.9	0.16259E+06	.8
36	9555.4	10059.2	0.80952E+05	1.5	0.10176E+06	.9	0.13970E+06	.8
37	10059.2	10603.8	0.72118E+05	1.5	0.87120E+05	1.0	0.12283E+06	.8
38	10603.8	11194.0	0.44732E+05	1.9	0.61627E+05	1.1	0.78463E+05	1.0
39	11194.0	11834.8	0.10323E+05	4.0	0.26208E+05	1.7	0.26636E+05	1.7

Table 1: Continued

Neutron Flux in neutrons/(sr . keV . microC) with Random Error in %

Group	Energy Range (keV)		20 deg		30 deg		45 deg	
1	798.1	1002.0	0.63859E+06	1.0	0.54673E+06	.8	0.41069E+06	.9
2	1002.0	1203.7	0.64678E+06	.7	0.53797E+06	.6	0.39362E+06	.7
3	1203.7	1416.0	0.63127E+06	.6	0.49382E+06	.6	0.35823E+06	.6
4	1416.0	1620.0	0.64641E+06	.6	0.47511E+06	.6	0.34840E+06	.6
5	1620.0	1816.7	0.64311E+06	.6	0.46458E+06	.6	0.32660E+06	.6
6	1816.7	2019.8	0.63575E+06	.6	0.45632E+06	.6	0.31813E+06	.6
7	2019.8	2222.2	0.62670E+06	.6	0.43637E+06	.6	0.30023E+06	.6
8	2222.2	2435.8	0.59684E+06	.6	0.40517E+06	.5	0.27822E+06	.6
9	2435.8	2634.3	0.56877E+06	.6	0.38688E+06	.6	0.27179E+06	.6
10	2634.3	2831.8	0.54489E+06	.6	0.37188E+06	.6	0.25079E+06	.7
11	2831.8	3052.5	0.52535E+06	.6	0.34857E+06	.6	0.23351E+06	.6
12	3052.5	3267.4	0.48860E+06	.7	0.32544E+06	.6	0.21794E+06	.7
13	3267.4	3470.2	0.46285E+06	.7	0.30550E+06	.6	0.20146E+06	.7
14	3470.2	3692.4	0.42354E+06	.7	0.28500E+06	.6	0.19269E+06	.7
15	3692.4	3894.4	0.41096E+06	.8	0.27399E+06	.7	0.17820E+06	.8
16	3894.4	4113.4	0.40163E+06	.8	0.26218E+06	.7	0.16470E+06	.8
17	4113.4	4302.2	0.37363E+06	.8	0.25118E+06	.8	0.14206E+06	.9
18	4302.2	4504.3	0.36868E+06	.8	0.22790E+06	.8	0.13353E+06	.9
19	4504.3	4720.9	0.33148E+06	.9	0.20052E+06	.8	0.12105E+06	1.0
20	4720.9	4953.6	0.32514E+06	.9	0.19234E+06	.8	0.10579E+06	1.0
21	4953.6	5203.9	0.27898E+06	.9	0.15061E+06	.9	0.10168E+06	1.0
22	5203.9	5404.3	0.20834E+06	1.2	0.12675E+06	1.1	0.10309E+06	1.1
23	5404.3	5616.6	0.19095E+06	1.2	0.12990E+06	1.1	0.98684E+05	1.1
24	5616.6	5841.5	0.19345E+06	1.2	0.13640E+06	1.0	0.86633E+05	1.2
25	5841.5	6080.3	0.18490E+06	1.2	0.12548E+06	1.1	0.84295E+05	1.2
26	6080.3	6333.9	0.13268E+06	1.4	0.11529E+06	1.1	0.83271E+05	1.2
27	6333.9	6603.8	0.12607E+06	1.4	0.11767E+06	1.1	0.83699E+05	1.2
28	6603.8	6891.4	0.12884E+06	1.4	0.12394E+06	1.0	0.86917E+05	1.1
29	6891.4	7198.1	0.13877E+06	1.3	0.13103E+06	1.0	0.85605E+05	1.1
30	7198.1	7525.8	0.15267E+06	1.2	0.14178E+06	.9	0.78419E+05	1.1
31	7525.8	7876.3	0.15831E+06	1.1	0.14481E+06	.9	0.76374E+05	1.1
32	7876.3	8252.0	0.16359E+06	1.1	0.15317E+06	.8	0.73954E+05	1.1
33	8252.0	8655.1	0.18074E+06	1.0	0.15903E+06	.8	0.68026E+05	1.1
34	8655.1	9088.6	0.18463E+06	1.0	0.15796E+06	.8	0.55540E+05	1.2
35	9088.6	9555.4	0.17258E+06	1.0	0.14527E+06	.8	0.45865E+05	1.3
36	9555.4	10059.2	0.14718E+06	1.0	0.12254E+06	.8	0.37225E+05	1.4
37	10059.2	10603.8	0.12971E+06	1.1	0.10065E+06	.9	0.22490E+05	1.8
38	10603.8	11194.0	0.75432E+05	1.3	0.57079E+05	1.1	0.76821E+04	3.1
39	11194.0	11834.8	0.20762E+05	2.5	0.12875E+05	2.4	0.55563E+03	17.2

Table 1: Continued

Neutron Flux in neutrons/(sr . keV . microC) with Random Error in %

Group	Energy Range (keV)		53 deg		68 deg		75 deg	
1	798.1	1002.0	0.36429E+06	1.6	0.27644E+06	1.3	0.25438E+06	1.1
2	1002.0	1203.7	0.34764E+06	1.3	0.29365E+06	1.0	0.27290E+06	.8
3	1203.7	1416.0	0.31763E+06	1.1	0.27882E+06	.8	0.26102E+06	.7
4	1416.0	1620.0	0.31677E+06	1.0	0.26166E+06	.8	0.24134E+06	.7
5	1620.0	1816.7	0.29042E+06	1.1	0.24993E+06	.8	0.22810E+06	.7
6	1816.7	2019.8	0.28775E+06	1.0	0.23953E+06	.8	0.22011E+06	.7
7	2019.8	2222.2	0.27157E+06	1.0	0.22629E+06	.8	0.20312E+06	.7
8	2222.2	2435.8	0.25722E+06	1.0	0.20905E+06	.8	0.18573E+06	.7
9	2435.8	2634.3	0.24328E+06	1.0	0.19026E+06	.9	0.16922E+06	.7
10	2634.3	2831.8	0.22254E+06	1.1	0.17201E+06	.9	0.15578E+06	.8
11	2831.8	3052.5	0.20863E+06	1.0	0.15878E+06	.9	0.14320E+06	.7
12	3052.5	3267.4	0.18877E+06	1.1	0.14913E+06	.9	0.13113E+06	.8
13	3267.4	3470.2	0.17658E+06	1.2	0.13782E+06	1.0	0.11859E+06	.8
14	3470.2	3692.4	0.16036E+06	1.2	0.12147E+06	1.0	0.10312E+06	.9
15	3692.4	3894.4	0.14821E+06	1.3	0.10695E+06	1.1	0.96801E+05	.9
16	3894.4	4113.4	0.13043E+06	1.3	0.98620E+05	1.1	0.80596E+05	1.0
17	4113.4	4302.2	0.12107E+06	1.5	0.83232E+05	1.3	0.70111E+05	1.2
18	4302.2	4504.3	0.11151E+06	1.6	0.75892E+05	1.4	0.71408E+05	1.1
19	4504.3	4720.9	0.93650E+05	1.6	0.73139E+05	1.4	0.71163E+05	1.1
20	4720.9	4953.6	0.91664E+05	1.6	0.76405E+05	1.3	0.68134E+05	1.1
21	4953.6	5203.9	0.94841E+05	1.6	0.68017E+05	1.4	0.59771E+05	1.2
22	5203.9	5404.3	0.89005E+05	1.8	0.60445E+05	1.6	0.52492E+05	1.4
23	5404.3	5616.6	0.72412E+05	2.0	0.54246E+05	1.7	0.53569E+05	1.4
24	5616.6	5841.5	0.68870E+05	2.0	0.55869E+05	1.6	0.55255E+05	1.3
25	5841.5	6080.3	0.71438E+05	1.9	0.58232E+05	1.6	0.54315E+05	1.3
26	6080.3	6333.9	0.73362E+05	1.9	0.56348E+05	1.5	0.50583E+05	1.3
27	6333.9	6603.8	0.70960E+05	1.9	0.51933E+05	1.6	0.44445E+05	1.4
28	6603.8	6891.4	0.69396E+05	1.9	0.43566E+05	1.7	0.39768E+05	1.4
29	6891.4	7198.1	0.59526E+05	2.0	0.40064E+05	1.7	0.38305E+05	1.4
30	7198.1	7525.8	0.55822E+05	2.0	0.38855E+05	1.7	0.35467E+05	1.5
31	7525.8	7876.3	0.52366E+05	2.0	0.35383E+05	1.8	0.32869E+05	1.5
32	7876.3	8252.0	0.47371E+05	2.1	0.30145E+05	1.8	0.28028E+05	1.6
33	8252.0	8655.1	0.35614E+05	2.3	0.27326E+05	1.9	0.25279E+05	1.7
34	8655.1	9088.6	0.31104E+05	2.5	0.25037E+05	1.9	0.20854E+05	1.8
35	9088.6	9555.4	0.28248E+05	2.5	0.19341E+05	2.2	0.13242E+05	2.2
36	9555.4	10059.2	0.18636E+05	3.0	0.99870E+04	3.0	0.38423E+04	4.1
37	10059.2	10603.8	0.82970E+04	4.5	0.13026E+04	10.4	0.77439E+02	95.8
38	10603.8	11194.0	0.72773E+03	21.2	---		---	
39	11194.0	11834.8	0.34602E+03	36.1	---		---	

Table 1: Continued

Neutron Flux in neutrons/(sr . keV . microC) with Random Error in %

Group	Energy Range (keV)		83 deg		90 deg		100 deg	
1	798.1	1002.0	0.23648E+06	2.0	0.23435E+06	2.0	0.20933E+06	2.1
2	1002.0	1203.7	0.26030E+06	1.5	0.25446E+06	1.5	0.22647E+06	1.5
3	1203.7	1416.0	0.24326E+06	1.3	0.23340E+06	1.3	0.20717E+06	1.3
4	1416.0	1620.0	0.23204E+06	1.2	0.21192E+06	1.3	0.18883E+06	1.4
5	1620.0	1816.7	0.20948E+06	1.2	0.19917E+06	1.3	0.17187E+06	1.4
6	1816.7	2019.8	0.20727E+06	1.2	0.18576E+06	1.3	0.16428E+06	1.3
7	2019.8	2222.2	0.18596E+06	1.2	0.17550E+06	1.3	0.15108E+06	1.3
8	2222.2	2435.8	0.17110E+06	1.2	0.15374E+06	1.2	0.14085E+06	1.3
9	2435.8	2634.3	0.15684E+06	1.3	0.14704E+06	1.3	0.13078E+06	1.4
10	2634.3	2831.8	0.14632E+06	1.3	0.13734E+06	1.4	0.11740E+06	1.5
11	2831.8	3052.5	0.13222E+06	1.3	0.12446E+06	1.3	0.10444E+06	1.5
12	3052.5	3267.4	0.12182E+06	1.4	0.10796E+06	1.4	0.93359E+05	1.6
13	3267.4	3470.2	0.10717E+06	1.5	0.99240E+05	1.5	0.77520E+05	1.8
14	3470.2	3692.4	0.96786E+05	1.5	0.80579E+05	1.6	0.63672E+05	1.9
15	3692.4	3894.4	0.82066E+05	1.8	0.69756E+05	1.9	0.63765E+05	2.0
16	3894.4	4113.4	0.69324E+05	1.9	0.68502E+05	1.8	0.64215E+05	1.9
17	4113.4	4302.2	0.71495E+05	2.0	0.69327E+05	2.0	0.60993E+05	2.1
18	4302.2	4504.3	0.71378E+05	2.0	0.66981E+05	2.0	0.56905E+05	2.2
19	4504.3	4720.9	0.67573E+05	2.0	0.60810E+05	2.0	0.52266E+05	2.2
20	4720.9	4953.6	0.64870E+05	2.0	0.53296E+05	2.1	0.54174E+05	2.1
21	4953.6	5203.9	0.55857E+05	2.1	0.52782E+05	2.0	0.55934E+05	2.0
22	5203.9	5404.3	0.53811E+05	2.4	0.56796E+05	2.3	0.55595E+05	2.3
23	5404.3	5616.6	0.54497E+05	2.3	0.55059E+05	2.3	0.53340E+05	2.3
24	5616.6	5841.5	0.54330E+05	2.3	0.52822E+05	2.2	0.45190E+05	2.4
25	5841.5	6080.3	0.52444E+05	2.3	0.46743E+05	2.4	0.44154E+05	2.5
26	6080.3	6333.9	0.45174E+05	2.4	0.43574E+05	2.4	0.42395E+05	2.4
27	6333.9	6603.8	0.42684E+05	2.5	0.39380E+05	2.5	0.39542E+05	2.5
28	6603.8	6891.4	0.39734E+05	2.5	0.38478E+05	2.5	0.36856E+05	2.5
29	6891.4	7198.1	0.36091E+05	2.6	0.36091E+05	2.5	0.30903E+05	2.7
30	7198.1	7525.8	0.33670E+05	2.5	0.31922E+05	2.7	0.26845E+05	2.8
31	7525.8	7876.3	0.29349E+05	2.7	0.27383E+05	2.8	0.26194E+05	2.7
32	7876.3	8252.0	0.26426E+05	2.8	0.24425E+05	2.9	0.20836E+05	3.1
33	8252.0	8655.1	0.23791E+05	2.8	0.18582E+05	3.2	0.14800E+05	3.6
34	8655.1	9088.6	0.17315E+05	3.2	0.12174E+05	3.9	0.44124E+04	6.7
35	9088.6	9555.4	0.92606E+04	4.5	0.24223E+04	9.5	0.14906E+03	72.9
36	9555.4	10059.2	0.14255E+04	12.3	---		---	
37	10059.2	10603.8	0.14935E+03	83.9	---		---	
38	10603.8	11194.0	---		---		---	
39	11194.0	11834.8	---		---		---	

Table 1: Continued

Neutron Flux in neutrons/(sr . keV . microC) with Random Error in %

Group	Energy Range (keV)		110 deg		120 deg		130 deg	
1	798.1	1002.0	0.19631E+06	1.6	0.19324E+06	1.6	0.18133E+06	1.4
2	1002.0	1203.7	0.22036E+06	1.1	0.20872E+06	1.1	0.19838E+06	1.7
3	1203.7	1416.0	0.19139E+06	1.0	0.17744E+06	1.1	0.16412E+06	1.6
4	1416.0	1620.0	0.17725E+06	1.0	0.15966E+06	1.1	0.15509E+06	1.5
5	1620.0	1816.7	0.15510E+06	1.0	0.14755E+06	1.1	0.13347E+06	1.6
6	1816.7	2019.8	0.14996E+06	1.0	0.13646E+06	1.1	0.12903E+06	1.6
7	2019.8	2222.2	0.13804E+06	1.0	0.12708E+06	1.1	0.11846E+06	.6
8	2222.2	2435.8	0.12531E+06	1.0	0.11243E+06	1.1	0.10210E+06	1.6
9	2435.8	2634.3	0.11633E+06	1.1	0.10371E+06	1.1	0.92766E+05	1.8
10	2634.3	2831.8	0.10685E+06	1.1	0.93119E+05	1.2	0.88976E+05	1.8
11	2831.8	3052.5	0.93299E+05	1.1	0.83642E+05	1.2	0.67142E+05	1.9
12	3052.5	3267.4	0.80290E+05	1.2	0.63256E+05	1.4	0.57438E+05	2.1
13	3267.4	3470.2	0.62123E+05	1.4	0.57286E+05	1.5	0.54157E+05	2.2
14	3470.2	3692.4	0.60090E+05	1.4	0.56195E+05	1.4	0.49032E+05	2.2
15	3692.4	3894.4	0.61823E+05	1.4	0.53562E+05	1.6	0.46586E+05	2.4
16	3894.4	4113.4	0.56281E+05	1.4	0.48629E+05	1.6	0.40824E+05	2.5
17	4113.4	4302.2	0.49851E+05	1.7	0.43730E+05	1.8	0.50889E+05	2.5
18	4302.2	4504.3	0.49362E+05	1.6	0.53046E+05	1.6	0.58943E+05	2.2
19	4504.3	4720.9	0.55118E+05	1.5	0.56204E+05	1.5	0.59418E+05	2.2
20	4720.9	4953.6	0.56755E+05	1.5	0.61398E+05	1.4	0.62476E+05	2.1
21	4953.6	5203.9	0.60584E+05	1.4	0.59771E+05	1.4	0.59873E+05	2.0
22	5203.9	5404.3	0.56844E+05	1.6	0.56423E+05	1.7	0.56471E+05	2.4
23	5404.3	5616.6	0.51417E+05	1.7	0.52449E+05	1.7	0.53058E+05	2.4
24	5616.6	5841.5	0.50318E+05	1.7	0.49760E+05	1.7	0.47543E+05	2.5
25	5841.5	6080.3	0.46074E+05	1.7	0.46060E+05	1.8	0.44416E+05	2.6
26	6080.3	6333.9	0.41791E+05	1.7	0.42535E+05	1.8	0.36499E+05	2.8
27	6333.9	6603.8	0.36902E+05	1.8	0.34573E+05	2.0	0.35751E+05	2.7
28	6603.8	6891.4	0.31363E+05	2.0	0.31742E+05	2.0	0.34711E+05	2.8
29	6891.4	7198.1	0.30051E+05	2.0	0.30866E+05	2.0	0.32482E+05	2.8
30	7198.1	7525.8	0.26714E+05	2.1	0.28270E+05	2.0	0.26127E+05	3.0
31	7525.8	7876.3	0.23726E+05	2.1	0.25109E+05	2.1	0.19337E+05	3.5
32	7876.3	8252.0	0.18759E+05	2.4	0.15899E+05	2.6	0.32625E+04	9.3
33	8252.0	8655.1	0.85677E+04	3.5	0.26354E+04	7.0	0.31005E+03	50.3
34	8655.1	9088.6	0.52201E+03	23.4	0.48261E+03	23.4	---	
35	9088.6	9555.4	---		0.12111E+03	82.8	---	
36	9555.4	10059.2	---		---		---	
37	10059.2	10603.8	---		---		---	
38	10603.8	11194.0	---		---		---	
39	11194.0	11834.8	---		---		---	

Table 1: Continued

Neutron Flux in neutrons/(sr . keV . microC) with Random Error in %

Group	Energy Range (keV)		141 deg		155 deg	
1	798.1	1002.0	0.17536E+06	1.5	0.16281E+06	2.6
2	1002.0	1203.7	0.17428E+06	1.4	0.17473E+06	1.7
3	1203.7	1416.0	0.15391E+06	1.3	0.14730E+06	1.7
4	1416.0	1620.0	0.14074E+06	1.2	0.13267E+06	1.6
5	1620.0	1816.7	0.11929E+06	1.3	0.11626E+06	1.7
6	1816.7	2019.8	0.11079E+06	1.3	0.10440E+06	1.7
7	2019.8	2222.2	0.10430E+06	1.3	0.95612E+05	1.7
8	2222.2	2435.8	0.91506E+05	1.3	0.87395E+05	1.6
9	2435.8	2634.3	0.82996E+05	1.4	0.80934E+05	1.8
10	2634.3	2831.8	0.74998E+05	1.4	0.65054E+05	1.9
11	2831.8	3052.5	0.57132E+05	1.5	0.55422E+05	2.0
12	3052.5	3267.4	0.52028E+05	1.6	0.49558E+05	2.1
13	3267.4	3470.2	0.44757E+05	1.8	0.41172E+05	2.4
14	3470.2	3692.4	0.42339E+05	1.8	0.44185E+05	2.2
15	3692.4	3894.4	0.41785E+05	1.9	0.42237E+05	2.4
16	3894.4	4113.4	0.41196E+05	1.8	0.48963E+05	2.2
17	4113.4	4302.2	0.50004E+05	1.8	0.58032E+05	2.2
18	4302.2	4504.3	0.56468E+05	1.7	0.59555E+05	2.1
19	4504.3	4720.9	0.59975E+05	1.6	0.56747E+05	2.1
20	4720.9	4953.6	0.56648E+05	1.6	0.57792E+05	2.0
21	4953.6	5203.9	0.56849E+05	1.5	0.54968E+05	2.0
22	5203.9	5404.3	0.53747E+05	1.8	0.56439E+05	2.2
23	5404.3	5616.6	0.51620E+05	1.8	0.52183E+05	2.2
24	5616.6	5841.5	0.49564E+05	1.8	0.46457E+05	2.4
25	5841.5	6080.3	0.43194E+05	1.9	0.46976E+05	2.3
26	6080.3	6333.9	0.39868E+05	1.9	0.44781E+05	2.3
27	6333.9	6603.8	0.37999E+05	2.0	0.39732E+05	2.5
28	6603.8	6891.4	0.36804E+05	2.0	0.35078E+05	2.6
29	6891.4	7198.1	0.31893E+05	2.1	0.23459E+05	3.0
30	7198.1	7525.8	0.24786E+05	2.3	0.12141E+05	4.3
31	7525.8	7876.3	0.13326E+05	3.2	0.96000E+03	22.1
32	7876.3	8252.0	0.28057E+04	7.4	0.32625E+03	42.7
33	8252.0	8655.1	0.84747E+03	18.3	---	
34	8655.1	9088.6	0.39397E+03	30.9	---	
35	9088.6	9555.4	0.13975E+03	57.7	---	
36	9555.4	10059.2	---		---	
37	10059.2	10603.8	---		---	
38	10603.8	11194.0	---		---	
39	11194.0	11834.8	---		---	

[a] For blank entries no results are reported, but it can be assumed that the yields are either exactly zero on the basis of energetics, or are so small that they are consistent with zero within the experimental uncertainties. All indicated angles are in the laboratory system.

Table 1: Continued

Table 2: Effect of Anisotropic Neutron Emission from the E_d = 7 MeV $^{9}Be(d,n)^{10}B$ Thick-Target Reaction on Calculated Integral Neutron-Induced Reaction Cross Sections[a]

Reaction	θ_{max}: ~0°	2.5°	5°	7.5°	10°	15°	20°	30°	45°	60°
Flat σ	1.00	1.00	1.009	1.019	1.027	1.045	1.062	1.077	1.057	1.007
$^{58}Ni(n,p)^{58}Co$	1.00	1.00	0.998	0.999	0.999	0.997	0.996	0.994	0.999	1.021
$^{27}Al(n,p)^{27}Mg$	1.00	0.987	0.959	0.928	0.889	0.806	0.738	0.663	0.645	0.690
$^{63}Cu(n,\alpha)^{60}Co$	1.00	0.968	0.911	0.846	0.774	0.641	0.551	0.466	0.452	0.503
$^{60}Ni(n,p)^{60}Co$	1.00	0.971	0.916	0.852	0.782	0.651	0.560	0.474	0.457	0.506
$^{27}Al(n,\alpha)^{24}Na$	1.00	0.948	0.863	0.768	0.673	0.519	0.428	0.351	0.343	0.397

[a]The simulated experiment involves measurement of the integral-cross-section ratio for each of the indicated reactions to fast-neutron fission of ^{238}U. The values in the tables are ratios of the calculated results obtained using the presently-measured neutron-emission data to what is obtained when isotropic emission is assumed.

Table 3: Calculated Neutron Scattering from a Hypothetical Beryllium Target Assembly for the E_d = 7 MeV $^{9}Be(d,n)^{10}B$ Thick-Target Reaction[a]

Reaction	Scattering Correction (%)	
	Anisotropic[b]	Isotropic
Flat σ	1.6	4.6
$^{238}U(n,f)$	1.1	3.1
$^{58}Ni(n,p)^{58}Co$	1.0	2.2
$^{27}Al(n,p)^{27}Mg$	0.9	1.7
$^{63}Cu(n,\alpha)^{60}Co$	1.0	1.5
$^{60}Ni(n,p)^{60}Co$	0.9	1.3
$^{27}Al(n,\alpha)^{24}Na$	0.8	1.1

[a]Beryllium target is centered in a copper beam stop which is 7.0 cm in diam and 0.2-cm thick, with a 2.0-cm-diam recess to 0.05-cm thickness in the vicinity of the beam spot. Scattering from the Beryllium is neglected.

[b]Anisotropy is consistent with the results of the present experiment.

FIGURE CAPTIONS

Figure 1: Schematic diagram of the experimental arrangement employed for the $^{9}Be(d,n)^{10}B$ thick-target spectrum measurements at E_d = 7 MeV. Three detectors were employed. The primary detector (D_1) was free to move in the range 0-155°. The two secondary monitor detectors (D_5 and D_8) were placed at 61.5° and 107.5°, respectively. Detector D_1 was a small (2.54-cm diam x 0.635-cm thick) NE-102A plastic scintillator. It generally viewed the beryllium target through an open collimator. Detectors D_5 and D_8 were larger (12.7-cm diam x 2.0-cm thick) NE-213 liquid scintillators. They each viewed the beryllium target through collimators which were blocked with lucite plugs to reduce the neutron fluences at these monitors. Inactive detector assemblies were placed around D_5 and D_8 to improve the shielding.

Figure 2: Schematic diagram of the beryllium target assembly used in the present work. An aperture (A) served to reduce the deuteron beam (d) intensity on the beryllium target (T) to manageable levels. The target components are assembled with insulators (I) so that the beam currents on the target and the aperture can be monitored separately. The walls of the target assembly (excluding flanges) are 0.05-cm thick to minimize neutron absorption and scattering. Two different target caps are used. Be 90 is used for measurements at forward and backward angles while Be 45 is used for measurements near 90°. The beryllium targets are 0.05 cm thick wafers of metallic beryllium which are fastened to the target end caps with electrically-conducting epoxy. These end caps are fabricated from 0.05-cm-thick stainless steel or tantalum.

Figure 3: Ratio of fast-neutron events from tantalum targets to those from beryllium targets bombarded with 7-MeV deuterons vs. laboratory angle.

Figure 4: Comparison of the experimental (-) efficiency shape and the calculated (---) efficiency shape for detector D_1, as discussed in Section 3. The normalization of the calculated curve was adjusted graphically to minimize the differences between the two curves. Neither curve is shown on an absolute scale.

Figure 5: Energy-group neutron spectra for the $^{9}Be(d,n)^{10}B$ thick target reaction at E_d = 7 MeV. The plots correspond to the results in Table 1. Although the absolute neutron yields in $n.sr^{-1}.keV^{-1}.\mu C^{-1}$ are not indicated, a consistent normalization is used for plotting the results for each of the laboratory angles.

Figure 6: Laboratory-angle distributions of emitted neutrons, summed over the indicated neutron-energy ranges. These angular distributions are absolutely-normalized.

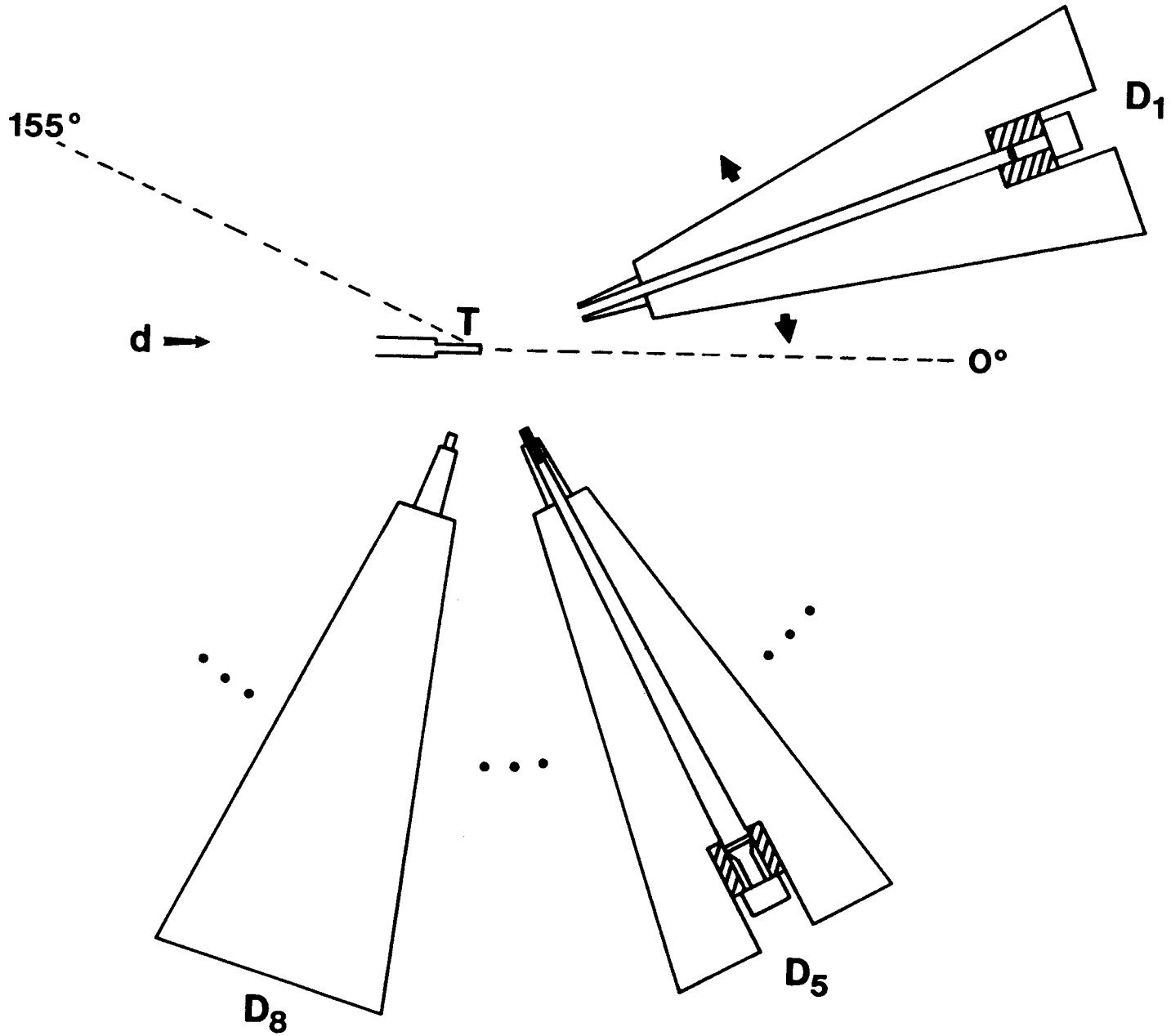

Figure 1

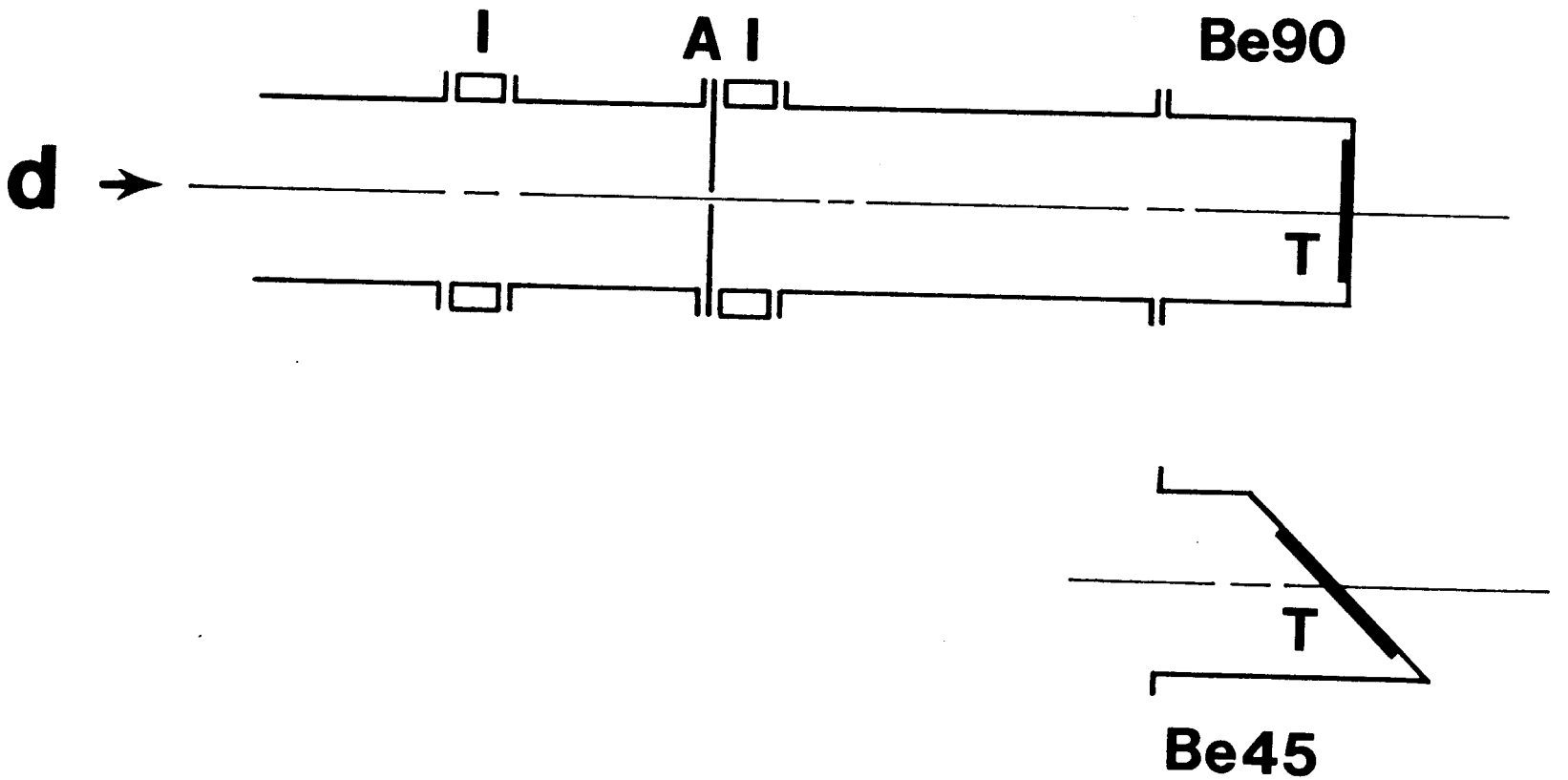

Figure 2

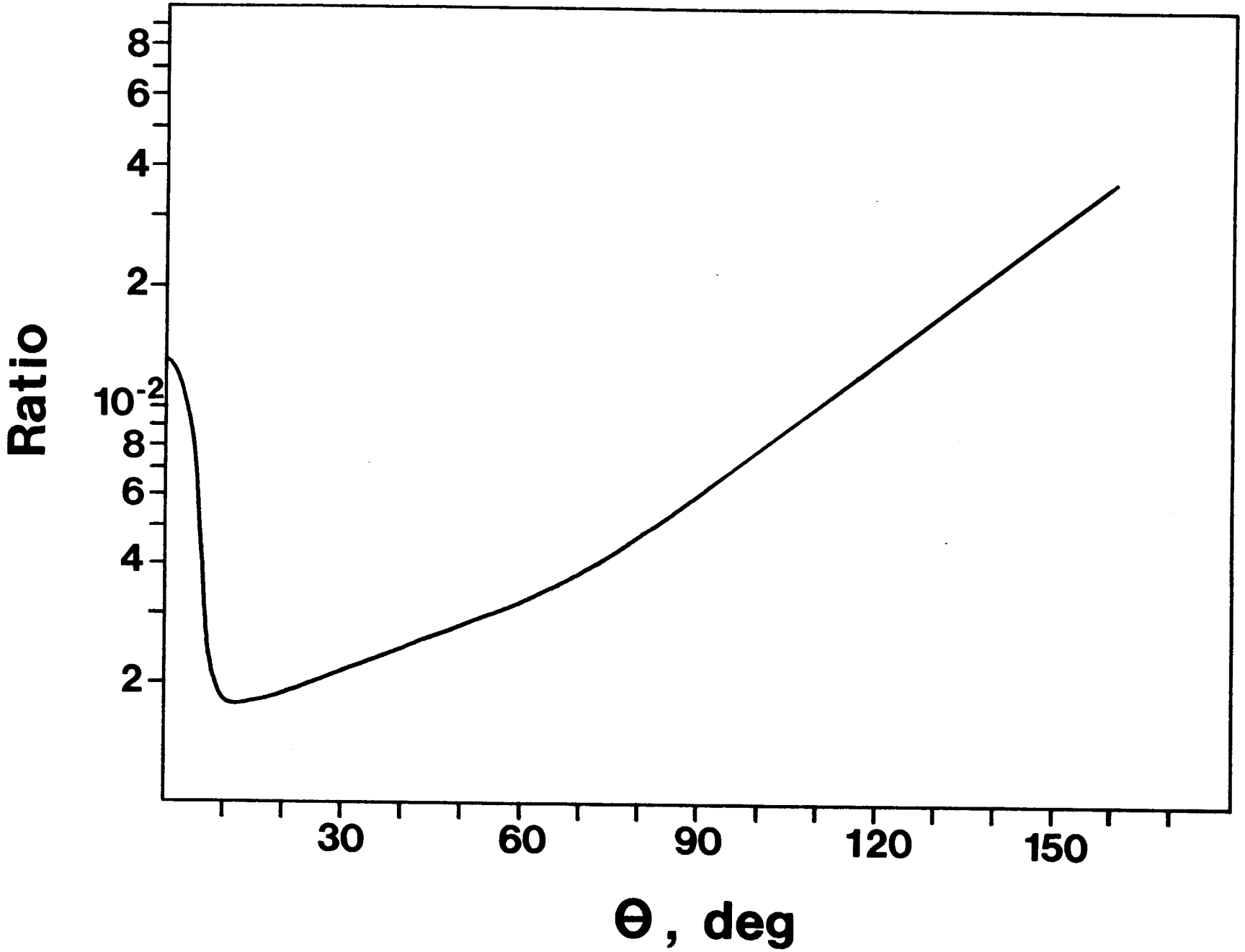

Figure 3

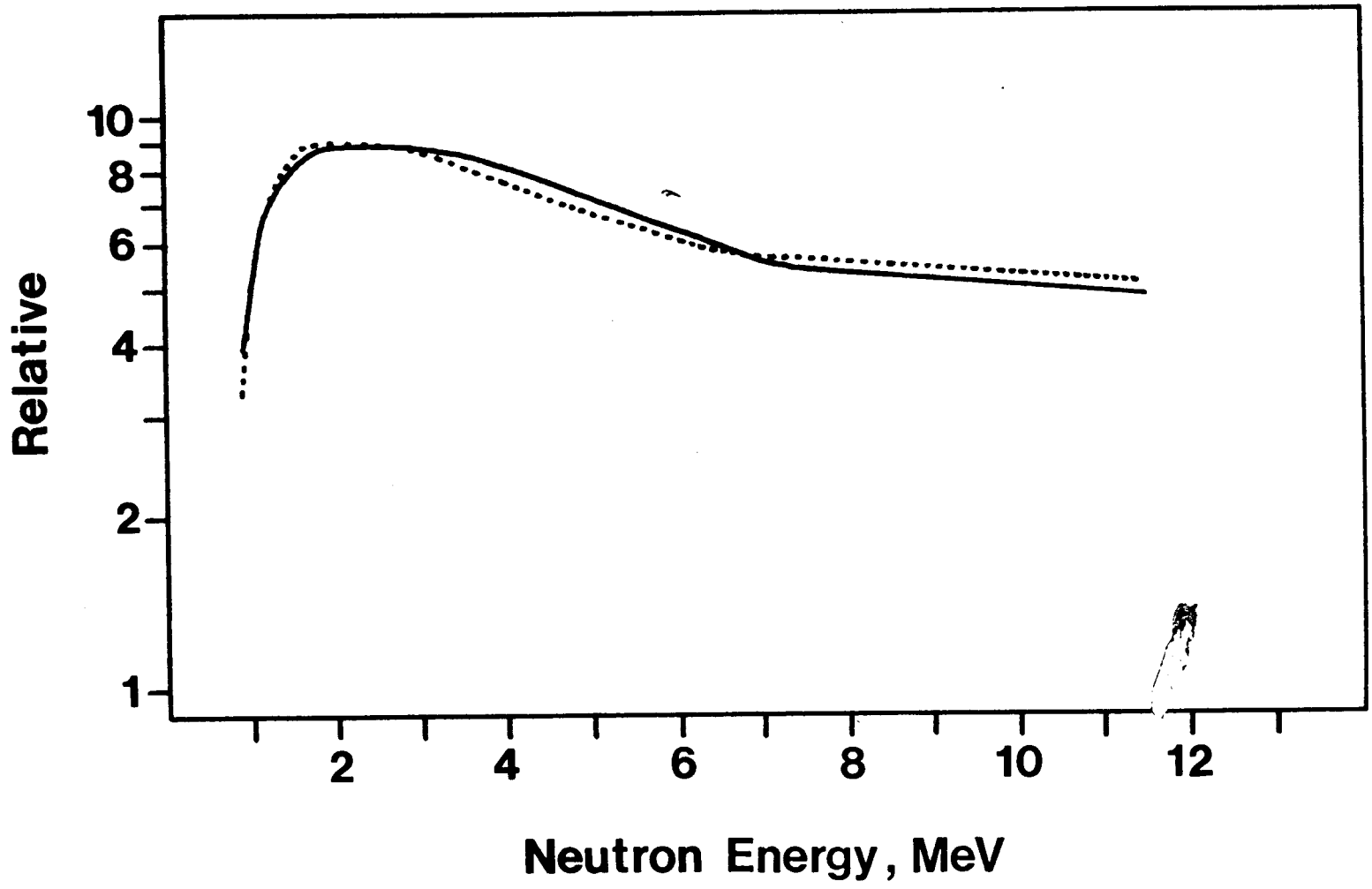

Figure 4

Figure 5

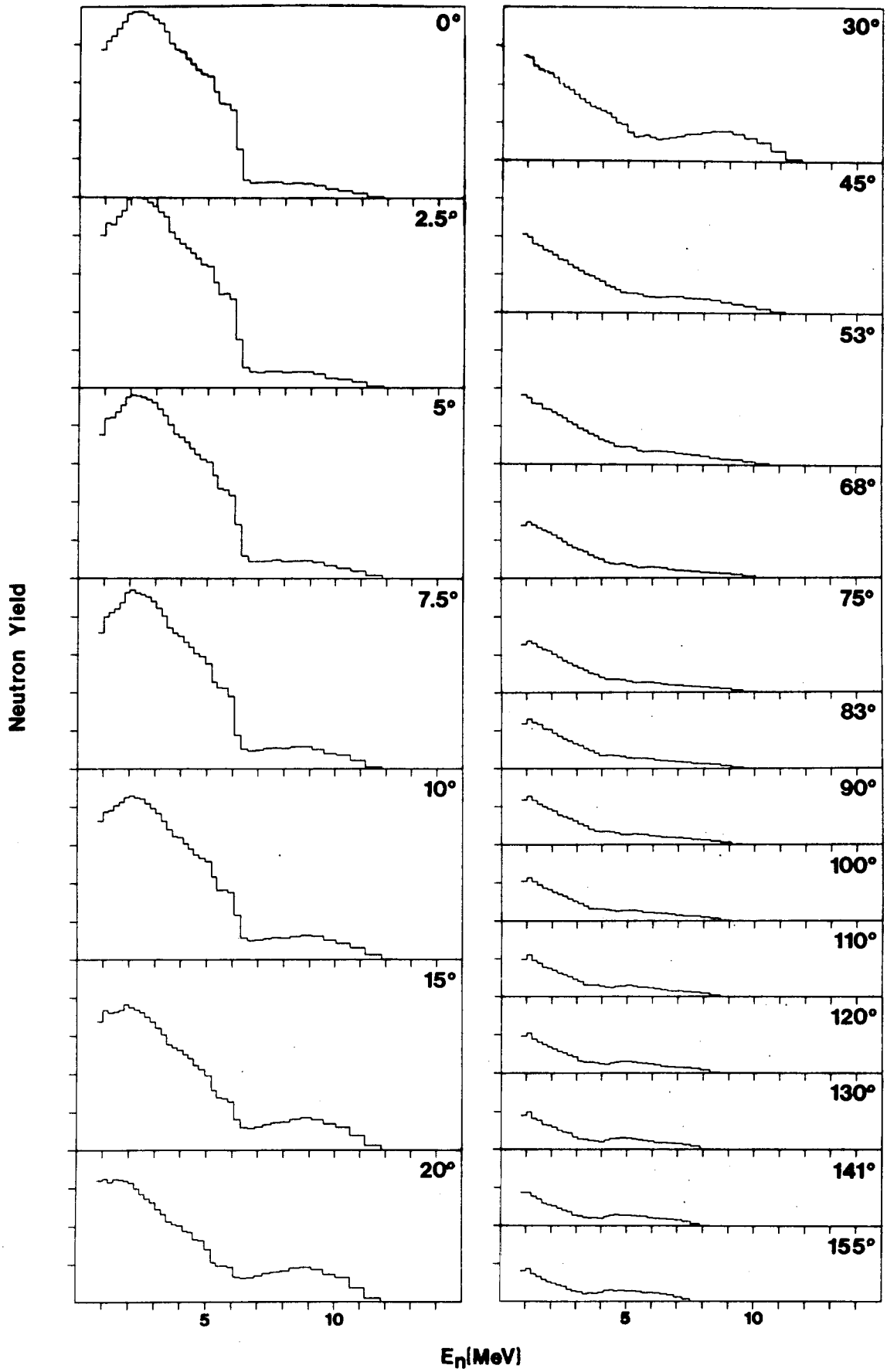
0°
2.5°
5°
7.5°
10°
15°
20°
30°
45°
53°
68°
75°
83°
90°
100°
110°
120°
130°
141°
155°
Neutron Yield
5
10
5
10
E_n(MeV)

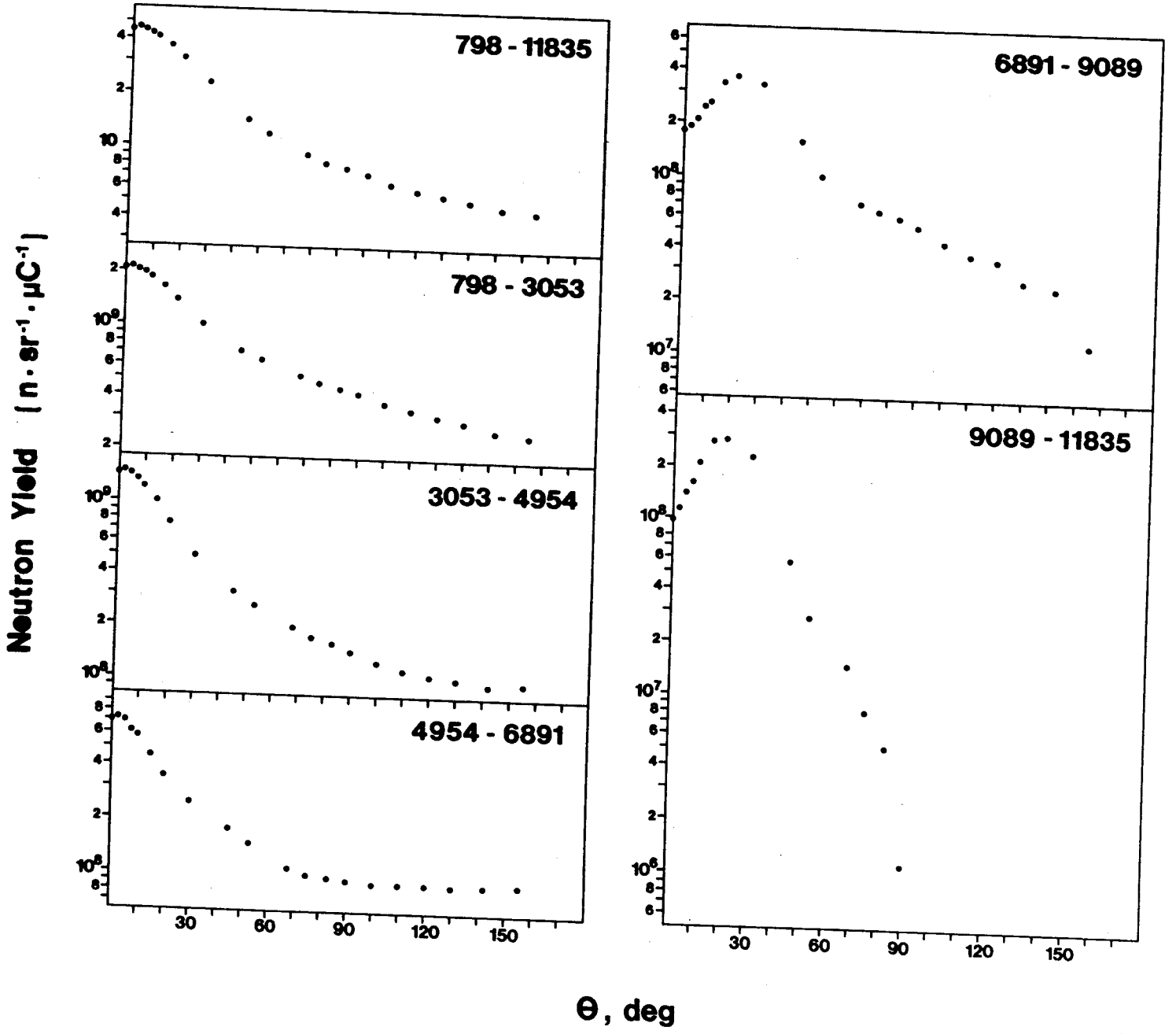
798 - 11835
798 - 3053
3053 - 4954
4954 - 6891
6891 - 9089
9089 - 11835
Neutron Yield [n · sr⁻¹ · μC⁻¹]
θ, deg
30
60
90
120
150

Figure 6